

# **Design and Development of a Wideband Coherent Radar Depth Sounder**

**By**

**Abhinay Kuchikulla**

B.E., Electronics and Communication Engineering,

Osmania University, 2001

Submitted to the Department of Electrical Engineering and Computer Science and the  
Faculty of the Graduate School of the University of Kansas in partial fulfillment of  
the requirements for the degree of Master of Science.

Thesis Committee

\_\_\_\_\_  
Chairperson: Sivaprasad Gogineni

\_\_\_\_\_  
Christopher Allen

\_\_\_\_\_  
Pannirselvam Kanagaratnam

Date of Defense: May 21<sup>st</sup>, 2004

# **ACKNOWLEDGEMENTS**

I would like to thank Dr. Prasad Gogineni for giving me an opportunity to work on this thesis, which is an imperative part of the PRISM project. I would like to thank him for his guidance throughout this thesis and for his suggestions and support during my graduate studies here at KU. I would like to thank Dr. Christopher Allen and Dr. Pannirselvam Kanagaratnam for their valuable suggestions during my research work and for serving on my thesis committee. I would like to express my appreciation for the support provided by NSF and NASA through Grant #OPP-0122520 (NSF) and Grant #NAG5-12659 and NAG5-12980 (NASA).

I would like to extend my sincere and utmost gratitude to Mr. Torry Akins and Mr. Saikiran Namburi for their invaluable guidance, advice, encouragement and inspiration throughout my thesis. I am greatly indebted to Mr. Torry Akins for guiding me towards being a better engineer. I take this opportunity to thank Ms. Kelly Mason for patiently editing my thesis report and helping me with managerial support. Special thanks to Mr. Dennis Sundermeyer for his time and effort in assembling the radar.

I would like to dedicate this thesis to my parents, Ramesh and Swarna for their endless love and support. This work would not have been possible without the strong support I received from my brother, Ajay. I would like to thank all the students in Remote Sensing Laboratory (RSL) for their help throughout my thesis. Finally, but not the least, I thank all my friends in Lawrence for the wonderful time I spent with them, which I will cherish for the rest of my life, GO Jayhawks.

## **ABSTRACT**

Sea level rise is an important indicator of global climate change. Sea level has been increasing at about 2mm/year over the past century and may continue to do so. The continuing rise in sea level will have a devastating impact on humanity as approximately 60% of people on this planet live in the coastal regions. The polar ice sheets, which account for 80% of earth's fresh water supply are a major source of sea level rise. A key to quantifying their contribution is an accurate determination of the mass balance of these ice sheets. Ice thickness is an important parameter required to estimate the mass balance of the ice sheet and to study ice dynamics. Depth sounding radars designed at RSL/KU have been successful in measuring the ice thickness for the past 10 years.

A Wideband Coherent Radar Depth Sounder System has been developed to obtain better delineation of the internal layers and information about the bedrock properties. The radar operates over a frequency range of 50-200 MHz, providing a resolution of less than 1 m in ice. A high speed Arbitrary Waveform Generator (AWG) is used to generate a chirp from 50-200 MHz over a very small pulse width to obtain large unambiguous range and the maximum number of integrations. Two gain channels are incorporated into the receiver to obtain very high dynamic range. The low gain channel is used to map the shallow internal layers and the HGC provides ice sheet thickness and bedrock properties up to a depth of 4500 m. The gain in both the channels can be altered depending on the operating mode, ice thickness, and

operating environment to obtain optimum performance. A high-speed data acquisition system is used to digitize and perform necessary real time processing on the data before transferring it to the storage device. The radar and data-acquisition systems have been significantly miniaturized using the latest RF and fabrication technology. The entire system has been designed to fit into multiple compact-PCI cards. Laboratory tests show that the radar system has the required sensitivity to map 4500-m-thick ice. Considerable improvement in sidelobe performance was achieved. The radar system will be tested during the Summer 2004 field experiment at Summit Camp, Greenland.

# Table of Contents

Chapter 1.....	1
<i>Introduction</i> .....	1
1.1 Motivation and Objectives of Studying Glacial Ice.....	1
1.2 Objectives of the PRISM project .....	3
1.3 Objectives, Approach and Overview of the report .....	5
Chapter 2.....	7
<i>Introduction to Ice Sounding Radars</i> .....	7
2.1 History of Radio-Echo Sounding.....	7
2.2 Work done at KU .....	10
Chapter 3.....	17
<i>Ice Sheet Model and System Parameters</i> .....	17
3.1 Introduction.....	17
3.2 Ice sheet model.....	17
3.3 Attenuation through Ice .....	18
3.4 Derivation of system specifications .....	25

Chapter 4.....	34
<i>Wideband Coherent Radar Depth Sounder</i> .....	34
4.1 System overview and operation .....	34
4.2 Control Signals and their Timing.....	38
4.3 Transmitter .....	39
4.4 Receiver .....	42
4.5 Frequency Synthesizer (10 MHz to 500 MHz).....	55
Chapter 5.....	59
<i>System Housing and Results</i> .....	59
5.1 WCORDS Prototype .....	59
5.2 System Housing .....	60
5.3 Results .....	63
Chapter 6.....	74
<i>Conclusions and Future Recommendations</i> .....	74
6.1 Conclusions.....	74
6.2 Future Recommendations .....	75

## List of Figures

Figure 3.1 Ice Sheet Model.....	18
Figure 3.2 Attenuation through ice at different acidic levels.....	24
Figure 3.3 Front end part of the Receiver affecting the noise figure of the system....	27
Figure 3.4 Low gain receiver chain .....	32
Figure 4.1 WCORDS Block diagram .....	35
Figure 4.2 WCORDS Timing .....	38
Figure 4.3 WCORDS Transmitter .....	39
Figure 4.4 Transmitter Schematic Diagram.....	41
Figure 4.5 Transmitter Board.....	41
Figure 4.6 WCORDS Receiver Front End.....	43
Figure 4.7 Front Bandpass Filter .....	44
Figure 4.8 Receiver Blanking Switch .....	45
Figure 4.9 Low Noise Amplifier.....	46
Figure 4.10 Bandpass Filter .....	47
Figure 4.11 Coupler (20 dB).....	47
Figure 4.12 Receiver Front End Schematic .....	48
Figure 4.13 Receiver Front End Board .....	48
Figure 4.14 High Gain Channel Block Diagram .....	49
Figure 4.15 High Gain Blanking Switch.....	49
Figure 4.16 Digital Attenuator.....	50
Figure 4.17 High Gain Amplifier.....	51

Figure 4.18 Final Amplifier .....	52
Figure 4.19 High Gain Channel Schematic .....	52
Figure 4.20 High Gain Channel Board .....	53
Figure 4.21 WOCRDS Low Gain Channel.....	53
Figure 4.22 Low Gain Channel Schematic .....	54
Figure 4.23 Low Gain Channel Board.....	54
Figure 4.24 10 MHz to 500 MHz Frequency Synthesizer .....	56
Figure 4.25 10-MHz to 500-MHz Frequency Synthesizer Schematic.....	57
Figure 4.26 10-MHz to 500-MHz Frequency Synthesizer Board.....	58
Figure 5.1 WCRDS Prototype and the final version.....	60
Figure 5.2 WCRDS modules mounted inside Aluminum compact PCI cards .....	62
Figure 5.3 Transmitter and Receiver compact PCI cards mounted inside Euro Cage	62
Figure 5.4 Transmitter Amplitude Response with Tx Blk ON.....	64
Figure 5.5 Transmitter Amplitude Response with Tx Blk OFF .....	64
Figure 5.6 Receiver Amplitude response with Rx and HG Blk OFF .....	65
Figure 5.7 Receiver Amplitude response with Rx Blk ON and HG Blk OFF .....	66
Figure 5.8 Receiver Amplitude response with Rx and HG Blk OFF .....	66
Figure 5.9 Receiver Transients .....	67
Figure 5.10 Transmit Chirp at the output of the AWG.....	69
Figure 5.11 Received Chirp at the output of the HGC .....	69
Figure 5.12 Received chirp and its Impulse response.....	71
Figure 5.13 Impulse response of ideal and recorded signals .....	71

Figure 5.14 Amplitude and Phase corrected transmit and received signal ..... 72

Figure 5.15 Impulse response of ideal, un-corrected and corrected signals ..... 72

## **List of Tables**

Table 2-1 Various time-domain radars used in radioglaciology.....	9
Table 2-2 System Parameters of CARDS, NGCORDS and ACORDS.....	13
Table 3-1 Compression Points of Front end components.....	33
Table 4-1 WCORDS System Parameters .....	37
Table 5-1 Amplitude of Transients generated due to switching.....	67
Table 5-2 Sidelobe performance.....	73
Table 5-3 Frequency Synthesizer performance .....	73

# Chapter 1

## *Introduction*

### 1.1 Motivation and Objectives of Studying Glacial Ice

In the last century, earth's average surface temperature rose by about 1° F. Also, the sea level has been increasing by about 2 mm per year due to expanding ocean water and the melting of temperate glaciers and polar ice sheets. Almost half of this rise in sea level has been attributed to ice loss from Greenland and Antarctica. It is important to understand and predict the net growth or shrinkage of ice sheet mass balance to quantify that contribution to present and future changes in sea level. Changing external conditions, such as atmospheric circulation patterns, significantly influence the mass balance of the ice sheet. Thorough knowledge of ice sheet internal properties, configuration and processes taking place deep in the ice are the keys in understanding the reasons for ice motion and ice thinning. It is predicted that continuous increase in sea level would lead to loss of wetlands along the southeast United States, eastern Mexico and southern Europe. But the regions where people will be most affected are south east Asia and Africa, which may result in massive migration of people [2]. If the Greenland ice sheet were to melt completely, sea level would rise by 7.6 meters [3]. But the temperature in Greenland would have to increase by 15°C to 20°C to get to an elevation where annual snowfall and melting

would be equal [3]. However, more recent studies suggest that the increase does not have to be as large as this.

There are two methods that scientists use for determining the mass balance of ice sheets, the component and the integrated. The component method involves estimation of the difference in annual mass input onto the ice sheet through snowfall and annual flux discharge from the ice sheet through surface melting and ice calving. The integrated method involves the determination of the change in volume of the ice sheet by measuring the change in surface elevation using radar and laser altimeters [3]. However, to understand the reasons for observed changes, other information such as spatial and temporal variation of accumulation is required. Knowledge of ice thickness, depth and shape of internal layers, subglacial topography and basal conditions will enable accurate measurement of boundary conditions, such as accumulation rate and the internal, dynamic processes that control ice sheet mass balance. Radar, operated in altimeter mode and referred to as sounders, are the least expensive, safest, and most effective method for measuring the ice thickness and internal structure of the ice sheet. Internal layers resulting from small changes in permittivity and conductivity represent isochrones and are useful in interpreting climate information.

Over the past decade, engineers at the Radar Systems and Remote Sensing Laboratory (RSL) at the University of Kansas have successfully developed depth sounding radars and have provided valuable ice thickness information from Greenland to the science community world wide. Advances in technology have led to

improvements in depth sounding radars, making them smaller, more efficient and more reliable. New and effective algorithms have been developed to process recorded data to obtain accurate information about the ice sheet, such as ice thickness, surface roughness, surface elevation, surface topology, ice accumulation, etc.

## 1.2 Objectives of the PRISM project

In 2001, a multi-disciplinary project, “Polar Radar for Ice Sheet Measurements (PRISM),” was initiated with grants from NASA and NSF. The project addresses the measurement of the ice sheet’s mass balance components and understanding of the internal, dynamic processes that control them. The goal of the project is to design and develop a sensor web for polar ice sheet measurements. The web will consist of ice-sheet-capable autonomous and intelligent rovers with radars for ice sheet measurement and sensors for navigation, hazard detection and communication [1]. Some of the primary objectives of the PRISM project are as follows:

- Develop a wideband dual-mode radar to measure ice thickness and map near-surface and deep internal layers with high resolution
- Develop a multiple-frequency Synthetic Aperture Radar (SAR) to measure basal conditions and determine whether the bed is wet or frozen, so as to predict the mode of glacier flow

- Develop automated rovers to support multiple radars and the sensor web with minimum human intervention, thus allowing the radars to be operated in harsh environments
- Develop networking and control capabilities for supporting the sensor web and provide automated collection and processing of data and transmittal of it to a central archive
- Develop various geophysical and electromechanical models of ice sheets based on recorded data
- Collect data over test sites in Greenland and Antarctica successfully

The PRISM project involves multidisciplinary groups working to achieve the goals mentioned above:

- Radar design and simulations
- Data analysis and visualization
- Wideband antenna design
- Robotics
- Information Systems

During the summer of 2003, prototypes and basic working concepts of all the radars, robotic rovers and networking wireless links were tested in northern Greenland at the North Greenland Ice Core Project camp (NGRIP), operated by the Danish government.

### 1.3 Objectives, Approach and Overview of the report

The primary objective of this project is to develop a Wide-Band Coherent Radar Depth Sounder (WCORDS) to meet the following PRISM project requirements:

- Measure the ice thickness up to a depth of 4km
- Obtain important information about ice sheet basal properties and scattering characteristics at different frequencies
- Map the deep internal layers with a range resolution of less than 1-2m in ice to estimate the history of past climate information and glacier deformation and also provide crucial validation of theoretical models
- Provide the flexibility of altering radar parameters to obtain optimum performance under different operating modes and environments
- Provide the ability to remove phase and amplitude nonlinearities of the system from the recorded data
- Miniaturize the radar system to fit into compact PCI cards
- Optimize the radar to be operated on both surface-based and airborne platforms

The approach was to first develop a fully operational prototype radar to validate the working of the concept and to check for any unseen errors and possible needs for improvement in and among the modules. This prototype was field tested during the 2003 field season. After the summer field experiment, an improved and miniaturized version of the Wideband Coherent Radar Depth Sounder was developed.

Chapter 2 covers a brief description of the history of Radio-Echo Sounding, followed by discussion of the work done at RSL and the recent depth sounders developed at RSL (NGCORDS and ACORDS), their limitations and problems, and advantages of WCORDS over them. Chapter 3 discusses the ice sheet model and losses associated with it. Derivation of important system parameters is also covered in the third chapter. Chapter 4 deals with the design and development of WCORDS and the 500-MHz frequency synthesizer required to support the digital system. Simulation and laboratory test results are included in Chapter 5. The concluding chapter covers future recommendations and suggestions to refine WCORDS.

## Chapter 2

### *Introduction to Ice Sounding Radars*

#### 2.1 History of Radio-Echo Sounding

The roots of Radio-Echo Sounding (RES) can be traced way back to 1933, when it was discovered at Admiral Byrd's base, Little America, Antarctica, that snow and ice appeared transparent to high-frequency radio signals. Later reports on the failure of radar altimeters over ice when operated in VHF and UHF bands led Waite and others to demonstrate in 1957 that a radar altimeter could be used to measure the thickness and other characteristics of polar glaciers [7, 8 and 9]. This development added a new chapter in the study of glaciology. Within 6 years after Waite's demonstration, the first of several VHF Radio-Echo Sounders was developed by Evans at Cambridge University's Scott Polar Research Institute (SPRI). The application of radio-echo sounding to glaciology generated interest among various research groups worldwide. During the 1960s and early 1970s, several research groups worldwide began developing and using first-generation RES systems. These RES systems operating between 30 MHz and 600 MHz, were successful in sounding ice sheets, glaciers and ice caps in Greenland and Antarctica. RES thickness estimates

when compared against results obtained from seismic and gravitational methods, agreed to within 2 percent [3 and 10].

By the mid 1970s, RES became one the most efficient and easiest methods for determining bedrock topography, ice thickness and internal layering. Initially, the RES systems were designed to estimate the ice thickness and layering information of the ice sheets, but soon it was realized that other important characteristics and features of polar ice could be estimated from the collected data. The second-generation of RES systems were designed to cater to a specific type of ice models, such as valley glaciers, cold thick ice sheets and warm ice sheets with liquid water present at the bottom. By the 1990s, with the advent of new technology and advancements in computing, digital systems, semiconductor devices and GPS systems, RES systems were becoming more compact, efficient and capable of relating data to a location with a resolution of 2-5 m. The third-generation RES systems were emerging to address specific glaciological questions. Table (2.1) provides a brief summary of various time-domain radar sets reported in the literature [5, 6, 7 and 11].

Year, System & Affiliation/ Country	Frequency (MHz)	Bandwidth (MHz)	Peak Power (W)	Pulse Width (us)	Range Accuracy (m)	System Performance (dB)	Source
1947, SCR-718, USA	440	3	7	0.5	20	128	Gogineni & others 1998 [7], Sinshemer 1947 [12]
1963, MARK-I SPRI/UK	35	14	80	0.3	5	127	Chuah 1996 [5], Raju 1989 [11], Gogineni & others 1998 [7], Walfold 1964 [13]
1964, IM4 USSR	213	1	50000-80000	2.5	60	180	Gogineni & others 1998 [7], Fedorov 1967 [14]
1967, USAEL/USA	30	3	200-400	0.5	20	150	Gogineni & others 1998 [7], Rinker & Mock 1967 [15]
1967, ADCOLE/USA	600	450	10	0.001	0.015	90	Gogineni & others 1998 [7], Evans 1967 [16]
1969, ANARE/USA	100	10	5000	0.3	7	173	Chuah 1996 [5], Raju 1989 [11], Evans 1970 [17], Gogineni & others 1998 [7]
1969, MARK-II SPRI/UK	35	14	800	0.24	10	160	Chuah 1996 [5], Raju 1989 [11], Evans & Smith 1969 [18], Jezek 1985 [19], Gogineni & others 1998 [7]
1978, MARK-II Univ of Iceland	2-10	3	8000	0.1	8	150	Chuah 1996 [5], Raju 1989 [11], Bjornsson & others 1977 [20], Sverrisson & others 1980 [21]
1980, UBC/Canada	840	40	4100	0.05	2.5	124	Chuah 1996 [5], Raju 1989 [11], Allen 1996 [22]
1982, RLS-620 USSR	620	15	820	1-0.1	---	146	Chuah 1996 [5], Raju 1989 [11], Allen 1996 [22]
1988, CARDS RSL/USA	150	17	20	1.6	5	186	Raju (1989, Thesis)
1996, ICARDS RSL/USA	150	17	200	1.6	5	196	Chuah 1996 [5],
1998, NGCORDS RSL/USA	150	17	200	1.6	5	200	Chuah 1996 [5],
1996, ACORDS RSL/USA	150	17	200	0.2 - 10	5	>200	Namburi (2003, Thesis)

**Table 2-1 Various time-domain radars used in radioglaciology**

## 2.2 Work done at KU

Ever since the formation of the Radar Systems and Remote Sensing Laboratory (RSL) in 1964, it has made a significant contribution to the field of remote sensing of the ocean, sea ice, snow, polar ice sheets, etc. The history of Depth Sounder Radars designed at RSL dates back to the 1980s when the Coherent Antarctic Radar Depth Sounder (CARDS) was developed using analog expansion and compression techniques along with post-digitized coherent averaging [5,11]. Even though CARDS had high loop sensitivity and high resolution with minimal transmit power, the theoretical and practical performance of the radar did not match. The errors in CARDS were recognized in a 1993 field experiment, and an enhanced version of CARDS, the Improved Coherent Antarctic and Arctic Radar Depth Sounder (ICARDS), was developed in 1996 and successfully tested in the field [5]. ICARDS, though successful, had connectorized components, which made it big and bulky, and also it used an old data acquisition system of CARDS. With the advent of new technology, low cost RFICs and MMICs were available with a wide selection of available IC specifications and smaller packages. This led to the development of a cheaper, smaller and superior version of ICARDS, the Next Generation Coherent Radar Depth Sounder (NGCORDS). A new data acquisition system with a 12-bit A/D was developed to complement the new NGCORDS. Since 1998, NGCORDS has been operating successfully, and the worldwide science community is using the data recorded by it [6]. In 2002-2003, multilayer FR4 boards and better surface mount components were used to develop the Advanced Coherent Radar Depth Sounder

(ACORDS). With its dual-channel receiver, ACORDS had a higher and properly controlled dynamic range. Generating the transmit signal digitally improved the loop sensitivity and removed the nonlinearities introduced by SAW devices.

### 2.2.1 NGCORDS

The success of NGCORDS lies in the fact that analysis of field experiment data collected during 1998-2002 provided ice thickness information over 90% of the region covered by it [6]. NGCORDS was unsuccessful in obtaining thickness over transition zones and a few glaciers in southern Greenland. The failure of NGCORDS in obtaining ice thickness over these regions has been attributed to multiple surface echoes and off-vertical surface clutter. NGCORDS transmits a 200-W linear chirp signal from 140-160 MHz over a pulse width of 1.6  $\mu$ sec. The received signal is amplified to an optimum value and then compressed before transforming it into in-phase and quadrature-phase baseband signals, after which the I and Q channel signals are captured digitally and stored using a data acquisition system with a 12-bit A/D. Signal expansion in the transmitter and compression in the receiver are done using Surface Acoustic Wave (SAW) devices. The dynamic range of the receiver is increased with a variable gain amplifier (VGA). Mixers are used to down-convert the compressed RF signal to baseband I and Q signals. The SAW devices, VGA and mixers introduced quite a bit of amplitude variations and phase nonlinearities into the system, which caused uneven sidelobe levels and deterioration of signal quality.

### 2.2.2 ACORDS

With rapid development of digital and analog ICs and fabrication techniques, the SAW devices, VGA and mixers were replaced in ACORDS with an Arbitrary Waveform Generator (AWG), dual channels in the receiver and a considerably higher-speed data acquisition system. These replacements provided the following advantages:

- The AWG directly generated a 140-160 MHz linear chirp over selectable pulse widths (0.2-10 $\mu$ sec). Generating the signal digitally using the AWG provided the flexibility to remove system effects from the transmit pulse
- Introduction of dual channels in the receiver eliminated the use of VGA and also increased the dynamic range of the receiver considerably
- High-speed data acquisition system sampling at 55 MHz allowed direct capture of the RF signal thereby eliminating mixers and phase shifter completely. Direct capture of raw data provided the flexibility of performing pulse compression digitally and applying various processing techniques to get better results

Considerable improvement in sidelobe levels, dynamic range and layering information was observed. ACORDS was quite successful in mapping the bedrock over most of the region covered by it. But it was unsuccessful in mapping outlet glaciers in southern Greenland. Table (2.2) summarizes the system parameters of ICARDS, NGCORDS and ACORDS [5,6 and 11].

Characteristics	ICARDS	NGCORDS	ACORDS
<b>RF Carrier Frequency (MHz)</b>	150	150	150
<b>RF Bandwidth (MHz)</b>	17	17	17
<b>Transmit Pulse Width (usec)</b>	1.6	1.6	0.2-10 (selectable)
<b>Range Sidelobes (dB)</b>	>26	>26	>36
<b>Receiver Dynamic Range (dB)</b>	90	93	>110
<b>Peak Transmit Power (Watts)</b>	200	200	200
<b>PRF (KHz)</b>	1.2, 2, 4.6, 9.2 (selectable)	2.3, 4.6, 9.2, 18.4(selectable)	Selectable
<b>Number of Coherent Integrations</b>	???	32-4096	32-1024
<b>Number of Incoherent Integrations</b>	1-64000	1-64000	1-64000
<b>A/D Dynamic Range (dB)</b>	8-bit, 48	12-bit, 72	12-bit, 72
<b>Noise Figure (dB)</b>	4	4	3.8
<b>Sampling Frequency (MHz)</b>	18.75	18.75	55
<b>Range Resolution in Ice (meters)</b>	4.494	4.494	4.494
<b>Antenna</b>	4-element $\lambda/2$ dipole array	4-element $\lambda/2$ dipole array	4-element $\lambda/2$ dipole array

**Table 2-2 System Parameters of CARDS, NGCORDS and ACORDS**

### 2.2.3 Limitations and problems with earlier radars

NGCORDS (1998 - 2003) and ACORDS (2003) were very successful in measuring ice thickness over most of the region they covered. But they had some

limitations and there was quite a bit of scope for improvement. Given below is a summarized list of limitations of NGCORDS and ACORDS

#### 2.2.3.1 NGCORDS

- Radar had to be operated over a limited frequency range, restricting the accurate measurement of scattering properties in ice and basal conditions
- Higher range sidelobes
- Lower receiver dynamic range
- Analog compression techniques introducing nonlinearities
- Time varying gain control, making it tough to keep track of returned signal power
- Mixers used in down conversion to IF introduced nonlinearities
- Entire radar and its power supply placed inside a huge rack mount chassis, which made the system heavy, big and bulky
- Poor range resolution of 4.494m, limiting the ability to accurately map the deep internal layers
- Radar had to be operated over limited frequencies and bandwidth

#### 2.2.3.2 ACORDS

- Radar had to be operated over limited frequency range restricting the accurate measurement of scattering properties in ice and basal conditions
- Poor range resolution of 4.494 m limiting the ability to accurately map deeper internal layers

- Radar had to be operated over limited frequencies and bandwidth
- Uneven and larger than ideal sidelobe levels caused due to amplitude and phase nonlinearities
- Used many control and power lines, making the system messy
- Though NGCORDS and ACORDS used surface mount components, each module in the radar had to be placed inside an RF-shielded enclosure to avoid coupling. All the modules and AC-DC power supply were placed inside a huge rack mount chassis, which made the system heavy, big and bulky
- Sampling a 20-MHz bandwidth signal at 55 MHz provides very little guard band and allow noise to couple into the signal band

#### 2.2.4 Advantages and improvements with the Wide Band Depth Coherent Radar Depth Sounder (WCORDS)

A Wideband Coherent Radar Depth Sounder (WCORDS) was developed to solve the limitations of existing radars and improve upon them. The radar developed would be able to operate over a partial or entire band from 50 MHz to 200 MHz. Operating the radar over the entire bandwidth would considerably reduce the range resolution to 55.9 cm, providing an accurate measure of deeper internal layers and basal properties. Scattering properties in ice over two octaves could be obtained. Operating the radar at lower frequency and wider bandwidth would probably reduce off-vertical surface clutter and obtain better data over outlet glaciers in southern

Greenland. The radar would be considerably miniaturized to fit inside compact PCI cards that would be placed inside a euro cage. Mounting the radar on a compact PCI chassis would improve grounding between various modules. WCORDS would have the following features

- Frequency of operation between 50 MHz and 200 MHz
- Amplitude and phase corrected transmit signal generated by an AWG
- Received data sampled at very high frequency (500MHz) in the DAC
- Dual channels in the receiver providing very high dynamic range
- Small and compact
- Eliminating limiter (surface-based applications) by providing a high-power and high-speed receiver blanking switch
- Including programmable CPLDs in the radar modules to reduce the number of control lines and also simplify the method of varying radar parameters

## Chapter 3

### *Ice Sheet Model and System Parameters*

#### 3.1 Introduction

Chapters 1 and 2 discussed previously developed radars and requirements for WCORDS. Chapter 3 describes a basic ice sheet model and its properties. The effects of temperature, density, acidity and scattering on signal attenuation are discussed. Ice loss over a wide range of frequencies is calculated using NGRIP temperature and density profile data to obtain an accurate estimate of signal attenuation over the operating frequency band. Receiver gain and other important radar parameters are calculated in the later portion of the chapter.

#### 3.2 Ice sheet model

As depicted in the figure, the top of the ice sheet is covered with a thin layer of snow, beneath which is ice that can be as thick as 4km. A very thin layer of water could be present between the ice and the bedrock. When a wave impinges on an interface between two media, the difference between the amplitude of reflected and transmitted signals depends on the ratio of dielectric constants of the two media. Thus, the amplitude of signal reflected from air-ice interface or ice-bedrock interface is larger

when compared to the reflections from internal layers where the change in dielectric constant is very small. A simple model of an ice sheet is shown in Figure [3.1].

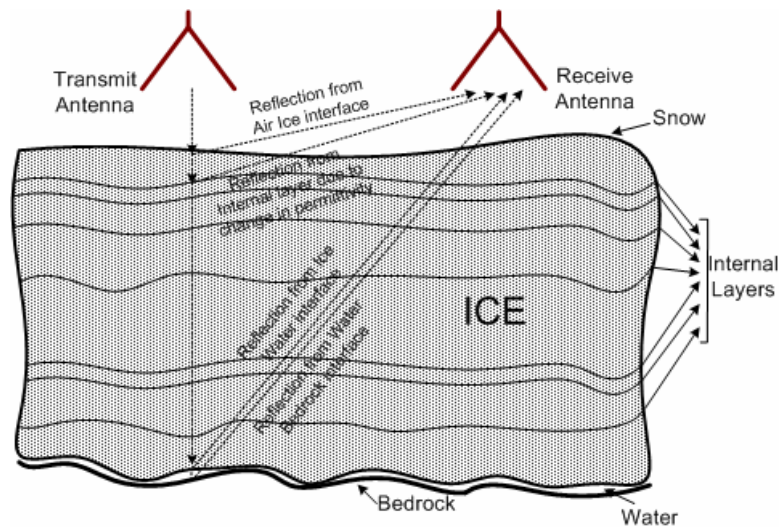


**Figure 3.1 Ice Sheet Model**

### 3.3 Attenuation through Ice

Ice sheets, being far away from population and pollution, have the purest form of naturally occurring ice known to humans, but events such as volcanic eruptions introduce dust particles into the ice over the years. Variation in climate and snowfall since the formation of the ice sheets cause the density and temperature of the ice to vary with depth. In order to get an accurate estimate of loss through ice, a close to ideal approximation of ice permittivity is required. Major factors affecting the variations in complex permittivity of ice are as follows:

- Temperature
- Density
- Acidity concentration and other impurities

This subsection deals with the estimation of attenuation through ice at NGRIP.

Wave equation for a source free media is given as [24]

$$\nabla^2 E_i + k^2 E_i = 0 \quad i = x, y, z. \quad (3.1)$$

Where wave number of the medium  $k = \sqrt{-j\omega\mu_0(\sigma + j\omega(\varepsilon' - j\varepsilon''))} \text{ m}^{-1}$

$\mu_0$  = Permeability of free space =  $4\pi \times 10^{-7}$  henrys/m

$\varepsilon' - j\varepsilon''$  = Permittivity of the medium

$\sigma$  = Conductivity of the medium

Considering electric field polarized in x direction

$$E = E_x(z) \hat{a}_x \quad (3.2)$$

Solving equation in

$$\frac{d^2 E_x}{dz^2} + k^2 E_x = 0 \quad (3.3)$$

Possible solution for the above homogeneous differential equation is given by,

[24]

$$E_x(z) = E_{x0}^+ e^{-z\gamma} + E_{x0}^- e^{+z\gamma} \quad (3.4)$$

Where  $\gamma = jk = \sqrt{j\omega\mu_0(\sigma + j\omega(\varepsilon' - j\varepsilon''))}$

From equation 3.4, accurate knowledge of complex permittivity and conductivity of the medium will enable us to calculate the signal attenuation in ice over various frequencies at constant depth or vice versa.

### 3.3.1 Effect of Temperature

Matzler and Wegmuller [23, 35] reported from their test results of polycrystalline ice at temperature above  $-30^{\circ}\text{C}$  and a frequency range between 2 GHz and 10 GHz that the real part of permittivity can be approximated as a linear function of temperature

$$\varepsilon' = (3.1884 + 9.1 \times 10^{-4}) \times T \quad (3.5)$$

Accurate results were obtained when the above equation was applied at MHz range. The imaginary part could be estimated as a summation of the Debye dispersion component and lattice vibration components [23,25 and 26].

$$\varepsilon'' = \frac{A}{f} + Bf^2 \quad (3.6)$$

The second part in equation 3.6 takes into account the effect of absorption due to lattice vibration, whereas the first term is an approximate form of the Debye expression for the imaginary part of complex permittivity of ice [23 and 27].

$$\varepsilon'' = \frac{(\varepsilon^0 - \varepsilon^\infty)}{1 + (2\pi f\tau)^2} 2\pi f\tau \quad (3.7)$$

Where  $\varepsilon^0$  = Relative static dielectric constant

$\varepsilon^\infty$  = Relative high-frequency limit dielectric constant

$\tau$  = Relaxation time

### 3.3.2 Effect of Density

The effect of density variation in ice can be incorporated into permittivity using an empirical formula suggested by Robin [28], based on field measurements made in Greenland:

$$\varepsilon_r = (1 + 0.851\rho)^2 \quad (3.8)$$

Where  $\rho$  = specific gravity of ice ( $g/cm^2$ )

Studies done by Tiuri [29] and Glen and Paren [30] revealed that the imaginary part of the permittivity increased with frequency. But the impact of this variation is negligibly small on signal attenuation and reflection.

### 3.3.3 Effect of Acidity

Conductivity arising due to the presence of acidity is the major cause of attenuation in ice. Fujita and others measured the variation in the real part of the dielectric constant using acid-doped polycrystalline ice and a network analyzer in the laboratory. The results closely matched with those from real ice core data. Based on the recorded data at different temperatures, they proposed an empirical formula with fitting parameters A and B [23]:

$$\frac{d\varepsilon'}{dC} = 10^A f^B \quad (3.9)$$

Variation in the imaginary part of the dielectric constant with frequency can be estimated using [23, 31 and 32]

$$\varepsilon'' = \frac{\text{acidity} \times S \times e^{\left[ \frac{-E}{R} \left( \frac{1}{T} + \frac{1}{253.15} \right) \right]}}{\frac{2\pi f}{\varepsilon_0}} \quad (3.10)$$

Where Molar conductivity of ice =  $S = 3.3(Sm^{-1}M^{-1})$

Molar Gas Constant =  $R = 8.31457(JK^{-1}mol^{-1})$

Permittivity of free space =  $\varepsilon_0 = 8.85 \times 10^{-12}(F/m)$

Frequency =  $f$  (Hz)

Activation Energy  $E = 0.22$  eV

$E(\text{Joules}) = N_A \times e \times E(\text{eV})$

Electron Charge =  $e = 1.6022 \times 10^{-19} C$

Avogadro's number =  $N_A = 6.02 \times 10^{23}$

Temperature =  $-20^\circ C$

### 3.3.4 Volume Scattering

Volume scattering in ice is caused due to the presence of discontinuities in the medium such as air bubbles or small spatial particles. When a signal traveling in a homogeneous medium encounters a sudden change in permittivity due to the presence of small foreign particles, the wave scatters in different direction. The magnitude and direction of scattering is dependent on the size, shape and relative permittivity of the particle. At lower frequencies, where the wavelength of the signal is high compared to the size of the discontinuous particles, scattering loss is negligible. The fraction of

power lost due to the presence of spherical discontinuous particles in the medium is given by [33 and 34]:

$$\delta = \frac{8\pi}{3} mb^6 \left( \frac{2\pi}{\lambda_0} \right)^4 \left[ \frac{\varepsilon_2(\varepsilon_1 - \varepsilon_2)}{\varepsilon_1 + 2\varepsilon_2} \right]^2 \quad (3.11)$$

Where  $m$  = Number of particles per unit volume

$b$  = Radius of the particles

$\varepsilon_1$  = Permittivity of the particle

$\varepsilon_2$  = Permittivity of the medium

Consider a case where spherical bubbles with a 1 mm radius are trapped inside a continuous medium of ice. Attenuation due to scattering can be derived from equation 3.11 [33] to be equal to:

$$L = \frac{5 \times 10^{-4}}{\lambda_0^4} \text{ dB per } 100\text{m} \quad (3.12)$$

At our highest frequency of operation (200 MHz), attenuation is calculated to be equal to  $98.77 \times 10^{-6} \text{ dB}/100\text{m}$ . This loss is negligibly small when compared to loss due to other effects.

Ice temperature and density profile data are available from the NGRIP drill site [31]. Though the data are not available down to the bedrock (3085 m), interpolating the available data will provide a close approximation of ideal results. Signal loss in ice due to temperature, density and acidity levels over a wide frequency band is plotted in Figure [3.2].

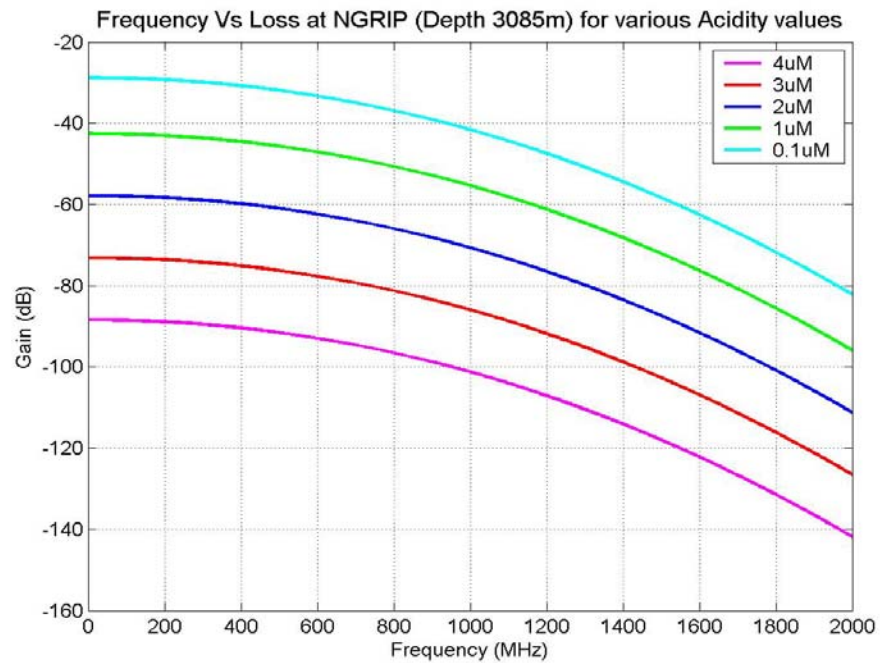


**Figure 3.2 Attenuation through ice at different acidic levels**

Two important things can be derived from the attenuation/frequency graph calculated using NGRIP data

- Acidity is a dominant factor in determining the effective loss through ice
- Over a frequency range from 10 MHz to 400 MHz, attenuation caused due to variation in density and temperature of ice can be considered to be constant

For the above data set spreading loss can be estimated as

$$\text{Spreading Loss} = 4\pi(2R)^2 = 4\pi(2 \times 3085)^2 = 87 \text{ dB}$$

Assuming scattering loss at the bedrock to be 10dB, and continuous acidity of 2uM through the ice, the total loss can be approximated to be equal to 157 dB.

### 3.4 Derivation of system specifications

Ideally, radar should be able to obtain all the required information about the target while transmitting a minimum amount of power. WCORDS is required to detect and differentiate multiple targets in the form of internal layers, top and bedrock. The amount of power reflected back from each of these targets primarily depends on the distance of the target from the source and the difference in dielectric constant between the layers. The dynamic range of the radar receiver should be large enough to record the high amplitude reflected signal from the top and shallow internal layers and also the very low amplitude reflection from the bedrock, which is at least 4km deep. A large dynamic range in the receiver can be achieved either by incorporating time varying gain into the receiver or splitting the receiver into multiple gain channels. Time-varying gain of the receiver introduces an element of error in estimating accurately the return signal power from each layer. Introduction of multiple channels in the receiver provides improvement in the dynamic range of the receiver and allows better control over overall receiver gain at the expense of multiple data acquisition systems.

From the previous section, the total loss through 3085-m ice at NGRIP was calculated to be close to 150 dB. In order to overcome such a huge ice loss, the radar would be required to have very large loop sensitivity, which can be achieved by transmitting a very large signal and/or designing a sensitive receiver. Some of the limitations encountered when transmitting high power signals are:

- Large power consumption

- High power amplifiers are costly, big and bulky
- Power amplifiers are limited by turn-on and turn-off times thereby restricting the radar to operate at narrow pulse widths
- Transmitting high power would require the transmitter and receiver antennas to be placed far apart to prevent the direct feed through signal from damaging the receiver
- Generally, a high-power amplifier generates large harmonics and spurious signals which might interfere with other communication systems operating in close vicinity
- Baluns or other impedance transformation devices used for antenna matching are big in size, costly and tough to manufacture when operated at high power

Hence, an optimum solution would be to design a sensitive receiver using a minimal amount of transmit power to obtain the required signal-to-noise ratio. Depending on the mode, bandwidth and characteristics of ice in the region of operation, the transmit power can be varied to get optimum performance. Post processing techniques such as coherent and incoherent integrations can be used to improve the signal quality. Gain required in both the gain channels depends on system parameters such as receiver noise, Analog to Digital Converter (ADC) noise level and signal processing gain.

### 3.4.1.1 System parameters

#### 3.4.1.1.1 Receiver Noise Floor

The amplitude of receiver noise floor is equal to the product of thermal noise and receiver noise figure:

$$N_{System}(dB) = N_{Thermal}(dBm) + NF_{Receiver}(dB) \quad (3.13)$$

Where Thermal Noise  $N_{Thermal} = KTB$  (Noise power at the antenna)

Boltzman Constant  $K = 1.38 \times 10^{-23} J / deg$

Equivalent Noise Temperature  $T = 290 K$

System Bandwidth  $B = 150 MHz$

$$N_{Thermal} = KTB = 600.3 \times 10^{-15} W = -92.21 dBm \quad (3.14)$$

Noise Figure of the receiver is calculated as

$$NF_{Receiver} = F_1 + \frac{(F_2 - 1)}{G_1} + \frac{(F_3 - 1)}{G_1 G_2} + \frac{(F_4 - 1)}{G_1 G_2 G_3} + \frac{(F_5 - 1)}{G_1 G_2 G_3 G_4} + \dots + \frac{(F_N - 1)}{\prod_{k=1}^{N-1} G_k} \quad (3.15)$$

Where  $F_N$  is noise figure of the  $N^{th}$  component from the front end of the receiver

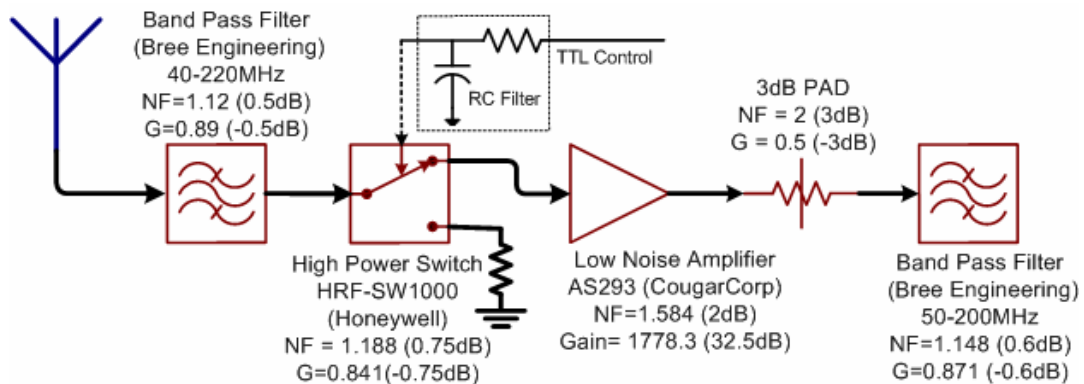


**Figure 3.3 Front end part of the Receiver affecting the noise figure of the system**

$$NF_{Receiver} = 1.12 + \frac{(1.188-1)}{0.89} + \frac{(1.584-1)}{0.89 \times 0.841} + \frac{(2-1)}{0.89 \times 0.841 \times 17784} + \frac{(1.148-1)}{0.89 \times 0.841 \times 17784 \times 0.5} + \dots$$

$$NF_{Receiver} = 1.12 + 0.211 + 0.78 + (0.75 \times 10^{-3}) + (0.22 \times 10^{-3}) + \dots$$

The noise added to the system by the components after the LNA is very small and can be ignored.

$$NF_{Receiver} = 2.11197 \text{ (or) } 3.246 \text{ dB}$$

$$N_{System} \text{ (dB)} = -92.21 \text{ dBm} + 3.246 \text{ dB} = -88.9674 \text{ dBm}$$

#### 3.4.1.1.2 ADC Noise Level

The WCORDS data acquisition system uses a high-speed 10-bit ADC to sample the data at 500Msps. The maximum allowable full-scale power level at the input of the ADC is determined by the maximum ADC input voltage and analog input terminating resistance. The ADC when operated in single-ended input mode can sample over a full-scale input voltage range from  $-250\text{mV}$  to  $250\text{mV}$ . The maximum signal the ADC can sample in a  $50\text{-}\Omega$  system is calculated as

$$P_{Max} = \frac{(V_{RMS})^2}{R} = \frac{(V_{PP}/(2\sqrt{2}))^2}{R} = \frac{V_{PP}^2}{8R} \quad (3.16)$$

$$P_{Max} = \frac{V_{PP}^2}{8R} = \frac{(0.5)^2}{8 \times 50} = 0.625 \text{ mW (or) } -2.04 \text{ dBm}$$

The ADC quantifies a continuous sinusoidal signal with a finite number of quantization levels. An error is introduced due to the difference in the actual analog signal level and its digitized counterpart. The signal-to-noise ratio for an ADC is given by:

$$SNR = \frac{3}{2} 2^{2B} = (6B + 10 \log_{10} 1.5) dB \quad (3.17)$$

Where B = Number of bits = 10

$$SNR = ((6 \times 10) + 1.761) dB = 61.761 dB \quad (49.76 \text{ dB, for 8 bits})$$

The noise level of the ADC is equal to the ratio of the maximum signal the ADC can sample to its SNR.

$$N_{ADC} = \frac{P_{Max}}{SNR} \quad (3.18)$$

$$N_{ADC} (dBm) = P_{Max} (dBm) - SNR (dB) = -2.04 - 61.761 = -63.801 dBm \quad (-51.8$$

dB, for 8 bits)

#### 3.4.1.1.3 Integration Gain

The thermal noise in the receiver is random in nature and can be estimated as being white. The signal amplitude remains constant when averaged but the noise amplitude goes down, thereby increasing the effective SNR. Also integrating the digital signal before storing reduces the storage space required. Noise is reduced by a factor of N for N coherent integrations and  $\sqrt{N}$  for N incoherent integrations. The number of pre-integrations can be selected by programming the data acquisition system accordingly. In both surface-based and airborne applications, 1000 coherent integrations is an acceptable number to start with.

$$\text{Integration Gain} = 10 \log_{10}(N) = 10 \log_{10}(1000) = 30 dB \quad (3.19)$$

#### 3.4.1.1.4 Pulse Compression Gain

Digital pulse compression using a match-filtering technique provides compression gain in post processing. The compression gain is equal to the product of the bandwidth and the transmit pulse width.

$$PCG = BT \quad (3.20)$$

$$PCG(dB) = 10\log_{10}(BT) \quad (3.21)$$

Where B = Bandwidth = 150 MHz

T = Transmit pulse width

For a 1usec pulse width, compression gain of 21.761 dB is obtained

#### 3.4.1.1.5 Strongest Received Signal

In surface-based applications, as the antennas are placed just a few meters above the ice, the signal returns from the air/ice interface and direct feed through signal arrive at the receiver antenna pretty much at the same time and are the strongest of all the reflections. The reflected power from the air/ice interface can be calculated as

$$P_r = \frac{P_t G_A^2 \lambda^2 \beta_a \beta_b \sigma^o}{64\pi^2 h^2} \quad (3.22)$$

Where  $P_t$  = Transmit Power = 50W (or) 47 dBm

$G_A$  = Antenna Gain = 3 dB (approx)

$\lambda$  = Wavelength (at center frequency 125 MHz) = 2.4m

$\beta_a$  = Antenna beamwidth in across-track direction = 70° [37]

$\beta_b$  = Antenna beamwidth in along-track direction = 30°

$\sigma^o$  = Backscattering coefficient of ice = -10 dB

$h$  = Height of antenna from ice = 1m

$$P_r (dBm) = P_t + 2G + 2\lambda + \beta_a + \beta_b + \sigma^o - 2h - 28$$

$$P_r (dBm) = 47 + (2 \times 3) + (2 \times 3.8) + 0.87 + (-2.81) + (-10) - (0 \times 2) - 28$$

$$P_r = 21.66dBm$$

### 3.4.1.2 Receiver Gain

#### 3.4.1.2.1 High-Gain Channel Gain

The purpose of High Gain Channel (HGC) is to detect the ice/bedrock interface and map the deep internal layers. Reflected signals from these layers have very small amplitude, and thus require considerable amplification to be detected by the data acquisition system. The amount of gain required in the high-gain channel should be such that, any signal present at the noise floor should be amplified to 10dB above the ADC noise level.

$$\text{ADC noise level (dBm)} + 10 \text{ dB} = \text{Rx noise floor (dBm)} + \text{Gain (dB)}$$

$$\text{Gain (dB)} = \text{ADC noise level (dBm)} + 10 \text{ dB} - \text{Rx noise floor (dBm)}$$

$$\text{Gain} = -63.801 \text{ dBm} - (-88.9674 \text{ dBm}) + 10 \text{ dB} = 35.1664 \text{ dB}$$

In the worse case of operation, out of 10 bits in the ADC only 8 bits could be effectively working, thus increasing the gain by 12 dB to give an effective gain of 47.1664 dB.

### 3.4.1.2.2 Low Gain Channel Gain

The purpose of the Low Gain Channel (LGC) is to detect the air/ice interface and map the shallow internal layers. The signal strength of the reflected signals from these layers is relatively strong and does not require a lot of amplification. Gain in this channel should not be in excess of what would be required to amplify the strongest reflected signal to saturate the amplifiers, digital attenuator and the ADC. The blanking switch at the front-end of the receiver attenuates the direct feed through signal and the top reflection to protect the receiver. The gain required in the LGC is first calculated such that the ADC never gets saturated.

$$\text{Gain (dB)} = \text{ADC Psat} - \text{Strongest received signal} + \text{Rx blanking switch isolation}$$

$$\text{Gain} = -2.04 - 21.66 + 50 = 26.3 \text{ dB}$$

Considering a gain of 26.3 dB in the LGC, the amplifiers and digital attenuator were selected such that none of them is saturated and to obtain maximum possible gain for optimum performance.

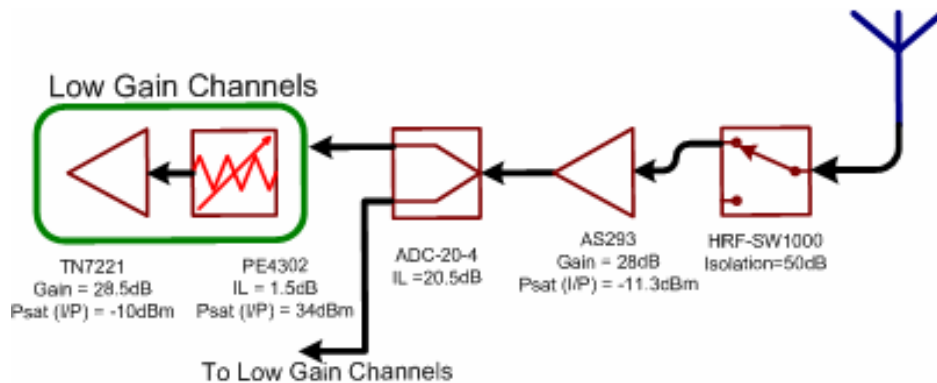


**Figure 3.4 Low gain receiver chain**

Components that have to be protected from saturating are tabulated in Table 3.1

COMPONENT	GAIN	SATURATION POWER (INPUT)
Low Noise Amplifier (AS293, Cougar Corp)	28 dB	-11.3 dBm
Digital Attenuator (PE4302, Perigrine Semi)	-1.5 dB	34 dBm
Amplifier (TN7221, Amplifonix Co)	28.5 dB	-10 dBm
ADC (TS83102G0B, Atmel)	-----	-2.04 dBm

**Table 3-1 Compression Points of Front end components**

### 3.4.1.3 Radar Loop Sensitivity

Radar's sensitivity to detect the smallest possible signal is defined by the loop sensitivity of the radar. It is defined as the ratio of peak transmit power to the minimum detectable signal. The minimum detectable signal is calculated as

$$MDS(dB) = N_{System}(dBm) + SNR(dB) - IG(dB) - PCG(dB) \quad (3.23)$$

$$\text{System Noise Floor} = N_{System}(dB) = -88.9674 \text{ dBm}$$

$$\text{Recorded SNR} = 0 \text{ dBm}$$

$$\text{Integration Gain} = IG = 30 \text{ dB (1000 coherent integrations)}$$

$$\text{Pulse Compression Gain} = PCG = 21.761 \text{ dB (1usec pulse width)}$$

$$MDS = -88.9674 - 0 - 30 - 21.761 = -140.728 \text{ dB}$$

$$\text{Loop Sensitivity (dB)} = \text{Peak transmit signal (dBm)} - MDS \text{ (dB)}$$

$$\text{Loop Sensitivity} = 47 - (-140.728) = 187.73 \text{ dB}$$

## Chapter 4

### *Wideband Coherent Radar Depth Sounder*

#### 4.1 System overview and operation

WCORDS is a frequency chirped pulse radar operating in the VHF and UHF bands to measure ice sheet thickness up to a depth of 4km and map deeper internal layers with a fine resolution of 56 cm. Basal properties and scattering characteristics can be obtained from the recorded data. The radar is designed to operate in both surface-based and airborne applications. Capturing the data directly enables the radar to be operated in chirp and step-frequency modes. A detailed block diagram of WCORDS is shown in Figure (4.1); the un-shaded region in the block diagram is the analog part of the radar.

##### 4.1.1 Transmitter

A highly stable, 10-MHz Rubidium reference oscillator with very low phase noise drives all the control and timing signals in the system. The transmit chirp signal of 50-200 MHz is generated using an AWG with selectable pulse widths. The frequency synthesizer provides a 500-MHz signal, which is phase locked to the 10-MHz reference oscillator. The AWG uses the phase-locked 500-MHz synthesizer signal as the clock signal to generate the 50-200-MHz chirp signal. Triggering and

control signals to determine the pulse repetition frequency (PRF), signal amplitude and other AWG characteristics are generated by the control unit that runs off the 10-MHz reference oscillator. The chirp signal is filtered for any unwanted noise signals generated by the AWG and then amplified to the optimum signal level by the transmitter module. The transmitter blanking switch provides better control over the signal pulse width and filters out any unwanted signals generated outside the transmitted pulse by the AWG. Combined reverse isolation of amplifiers and the transmitter blanking switch protect the transmitter and AWG from any unexpected high amplitude signals picked up by the transmitter antenna.

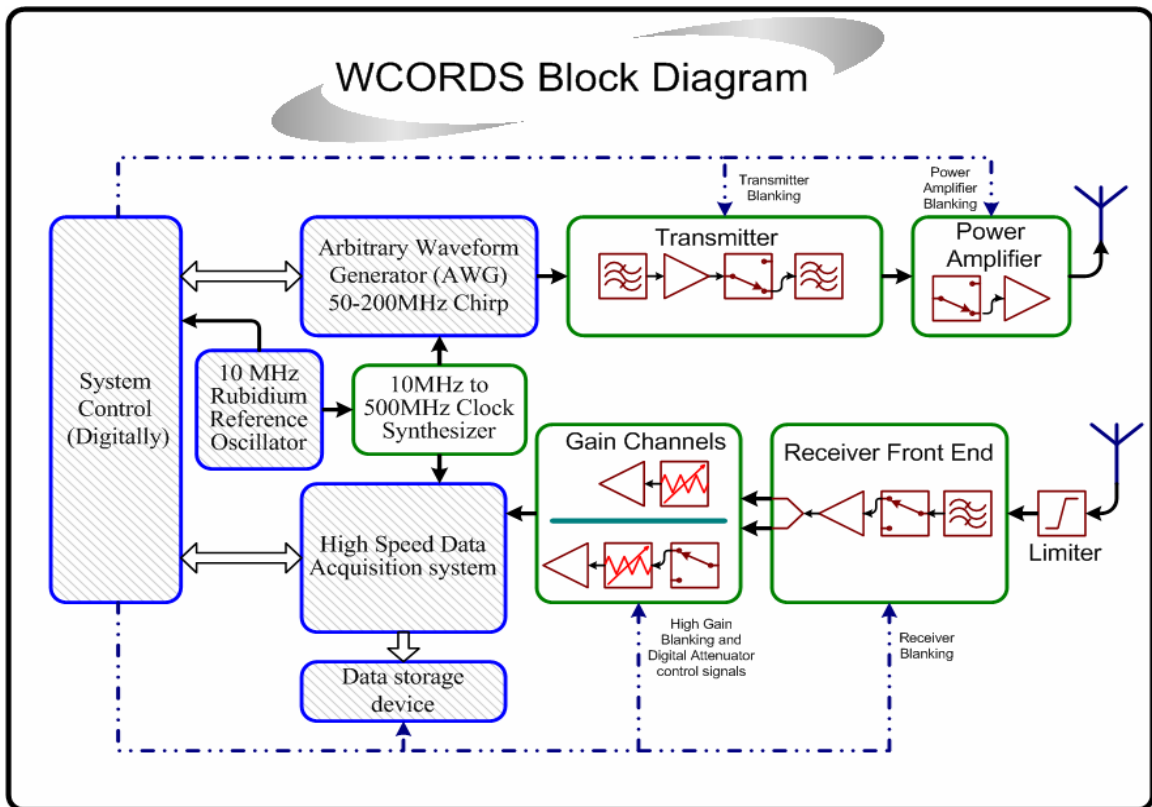


**Figure 4.1 WCORDS Block diagram**

### 4.1.2 Receiver

A high power receiver-blanking switch protects the receiver from the large direct feed through signal and reflections from the top and near-surface internal layers. The receiver consists of dual gain channels to obtain a high dynamic range. The high-gain blanking switch protects the high-gain channel from saturation and damaging while receiving large reflected signals. Digital attenuators provide gain adjustment in the receiver to obtain optimum performance under various working conditions. The digital system generates the control signals for all the blanking switches and digital attenuators. High-speed, 10-bit ADC sample the analog signal at 500 MHz. A de-multiplexer after the ADC slows the data rate by 4 times to make it easier to record and work with the data. The number of coherent and incoherent integrations, switching timing controls and digital attenuator bit vales are selectable and easily programmable. The high-speed data acquisitions system and digital control unit were designed and developed by Mr. Torry Akins.

The radar can be operated in between the range or entirely over a wide frequency band of 50 MHz to 200 MHz. In a noisy environment, the radar can be operated in step-frequency mode or over a selective bandwidth by just including external additional bandpass filters at the receiver input. The number of coherent and incoherent averages practically possible depend on the operational PRF, characteristics of ice (ice thickness, scattering characteristics, etc) in that region and the velocity of the vehicle on which the radar is mounted. Important WCORDS system parameters are tabulated in Table (4.1).

Parameters	WCORDS	Units
RF Center Frequency	125	MHz
RF Bandwidth (MHz)	150	MHz
Transmit Pulse Width	Selectable	usec
Range Sidelobes	Selectable, depending on the weighting used (>29 for Hanning)	dB
Receiver Dynamic Range	>114	dB
Peak Transmit Power	50 – 80 (Surface-based) 200 (Airborne)	Watts
PRF	Selectable	KHz
Number of Coherent Integrations	1000 (Selectable)	-
Number of Incoherent Integrations	Selectable	-
A/D Dynamic Range	>48 (10 Bits)	dB
Noise Figure	3.246	dB
Sampling Frequency	500	MHz
Range Resolution in Ice	55.9	cm
Antenna	Surface-Based – Bowtie Airborne- $\lambda/2$ dipole array	
High Gain channel gain variation	62	dB
Low Gain channel gain variation	31	dB

**Table 4-1 WCORDS System Parameters**

## 4.2 Control Signals and their Timing

The required transmit signal is fed into the AWG in the form of a waveform file. A narrow trigger pulse is required to make the AWG start generating the chirp. The ON time of the transmitter-blanking switch is equal to the transmit pulse width, but moved ahead in time to account for the finite delay from the AWG to the transmitter blanking switch.

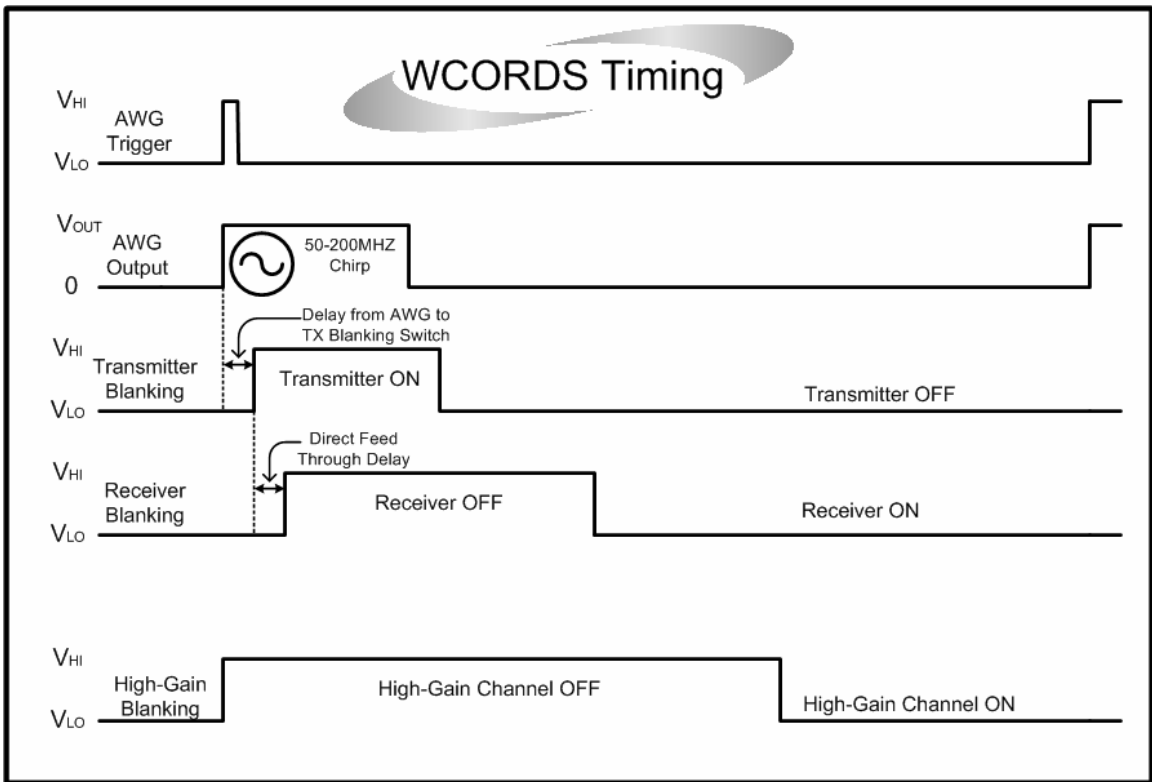


**Figure 4.2 WCORDS Timing**

While transmitting, the high-power receiver-blanking switch is switched off to avoid the receiver being driven into saturation by the direct feed through and the top reflection. The switch is also turned off even while receiving strong reflections from

near-surface internal layers and it is switched on only when the received signal power is just less than what would be required to saturate the LGC in the receiver. Similarly, as long as the signal power is high enough to saturate the HGC, the High-Gain blanking is switched off. As soon as the amplitude of the received signal level drops to a point where it doesn't saturate the HGC of the receiver any more, the High-Gain blanking is switched on. Both the blanking switches used in the receiver are absorptive and when switched off, they are terminated to ground through a 50-Ω impedance to minimize the reflected signal power.

### 4.3 Transmitter

The WCORDS transmitter can be divided into three phases

- Signal generation
- Signal conditioning
- Signal amplification

The block diagram of the WCORDS transmitter is shown in Figure (4.4)

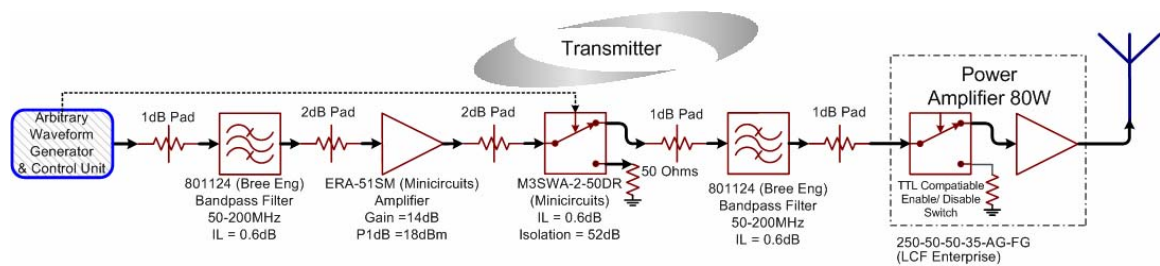


**Figure 4.3 WCORDS Transmitter**

A linear 50-MHz to 200-MHz chirp signal over a selectable pulse width is achieved using an AWG DBS 2050A manufactured by Analogic Corporation. The

required chirp waveform sampled at 500 MHz is generated using MATLAB and fed into the AWG in the form of a waveform file. A compact waveform generator using a Direct Digital Synthesizer (DDS) is being developed by Mr. Torry Akins to replace the AWG. The AWG is immediately followed by a bandpass filter to remove any unwanted out-of-band image frequencies, harmonics and other spurious signals that might interfere with other communication and radar systems operating in the radar's close vicinity. After passing through the filter, the signal is pre-amplified with a low power amplifier (Minicircuits ERA-51SM). The preamplifier was selected such that the gain and output saturation point of the amplifier were sufficient to drive the power amplifier to its maximum power. The preamplifier is followed by a single-pole-double-throw (SPDT) switch (Minicircuits M3SWA-2-50DR) with high isolation to reduce leakage signal. Even a small in-band signal generated by the waveform generator lying outside the pulse will get amplified to a considerable power level before being transmitted. Reflected signals from this transmitted leakage can be mistaken for low power signal reflections of actual signal from deep internal layers. The control signals for the high-isolation switch were setup such that the switch would be ON during the transmit pulse duration and OFF during the rest of the time period. Being an active component, the pre-amplifier and the switch would generate harmonics and other spurious signals like inter-modulation products and switching transients. A bandpass filter precedes the switch and preamplifier to remove any spurious signals generated by them. After going through the conditioning phase and pre-amplification, the signal is amplified to 50W (47 dBm) by a power amplifier

(LCF Enterprise 250-50-50-35-AG-FG). The power amplifier can be switched OFF when not transmitting thus blocking any unwanted signals outside the pulse duration.

The schematic and image of the transmitter board are shown below.

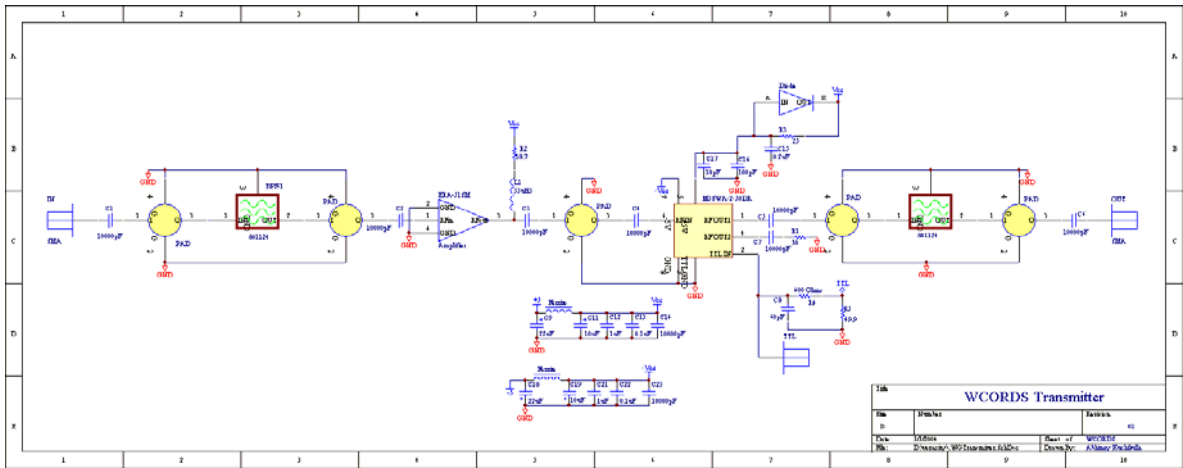


**Figure 4.4 Transmitter Schematic Diagram**

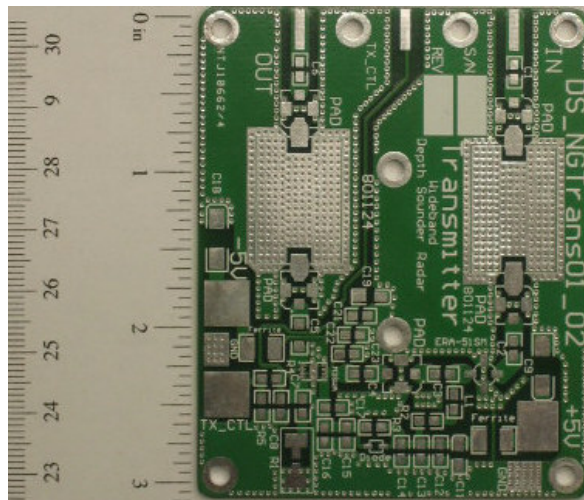


**Figure 4.5 Transmitter Board**

## 4.4 Receiver

The design of the WCORDS receiver was based on the gain calculations presented in Chapter 3, and given below is a summary of all the requirements that had to be satisfied.

- High dynamic range to detect both deep internal layers and bedrock clearly
- Effective gain in the HGC to be more than 48 dB
- Effective gain in the LGC to be more than 32 dB
- Minimum possible noise figure with optimum performance
- Ability to vary the gain of the receiver over a wide range
- Flat amplitude response and linear phase response over the entire band
- Front-end of the receiver should have high input return loss, thus minimizing the amplitude of signal reflected back through the transmitter antenna to generate a multiple
- Small and compact to fit into a single aluminum compact PCI card
- Providing ease of control

The WCORDS receiver was divided into three modules to provide good isolation and make the boards easy to design and debug for errors

- Front-end module
- Low Gain Channel
- High Gain Channel

#### 4.4.1 Front-end

The purpose of the front-end module of the receiver is to properly condition the received signal before feeding it into both channels. The characteristics, importance and purpose of important components in the front-end receiver chain are discussed in this section. The block diagram of the front-end module is shown below in Figure 4.6.

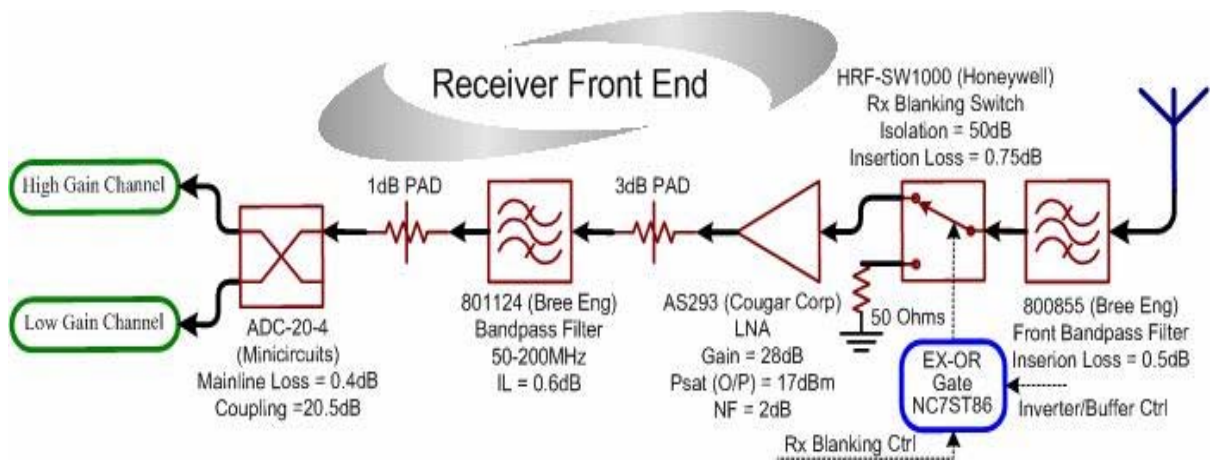


**Figure 4.6 WCORDS Receiver Front End**

#### Bandpass Filter (Wideband)

The signal received by the antenna is passed through a low-loss wideband bandpass filter to remove any out-of-band noise. The key parameters considered in selection of this filter are low passband insertion loss and high return loss over the entire band. Any insertion loss introduced by the filter adds up to the receiver noise figure. The input return loss of the filter should be considerably high over the range of 50 MHz to 200 MHz to minimize multiples. A bandpass filter with a wider pass-band from 37 MHz to 223 MHz was selected so that it provides at least 15 dB over the entire

bandwidth of 150 MHz. Selecting a wider pass-band would allow more noise to couple into the receiver, but this can be removed by using a bandpass filter with an exact pass-band later on in the receiver chain where insertion loss and reflections are a major concern.

800855 (Bree Engineering)

Passband Insertion Loss  $\leq 0.5$  dB

Input/Output Return Loss  $\geq 19.5$  dB

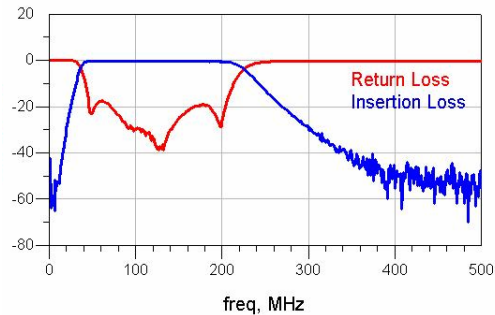


**Figure 4.7 Front Bandpass Filter**

#### Receiver Blanking Switch

The amplitude of the signals reflected from the top surface and shallow internal layers is large enough to saturate the receiver. A limiter at the front of the receiver can be employed to reduce the amplitude of these reflected signals. But a limiter not only adds extra loss in the front-end of the receiver but also generates harmonics by clipping the high amplitude signals. Introducing a low-loss, fast and high-power single-pole-double-throw (SPDT) blanking switch would allow us to attenuate the high amplitude signals considerably. After testing several switches, it was noticed that GaAs switches tend to get damaged when operated at low frequencies (50 MHz) and high power (25 dBm). A CMOS switch manufactured by Honeywell using silicon on insulator technology was selected as it worked well at 50 MHz and 27 dBm input power. The video leakage in the switch was considerably

smaller than that of GaAs switches, and it was small enough to avoid saturating the LNA. While receiving high amplitude signals, the switch is connected to a port that is terminated to ground through a 50-Ω load, thus minimizing the reflections. When the signal amplitude is not large enough to saturate the front end and LGC in the receiver, the switch is connected to the port that is in series with the receiver chain. The switch requires a CMOS level control signal to switch among the ports. Passing the control signal through an EX-OR gate transforms the TTL level signal to CMOS level and provides the flexibility of inverting the control signal. The transients introduced into the RF port from the control line are also considerably small, so as to saturate the LNA.

HRF-SW1000 (Honeywell)

Insertion Loss ON  $\leq 0.75$  dB

Isolation  $\geq 45$  dB

Input Return Loss ON  $\geq 23$  dB

Input Return Loss OFF  $\geq 18.5$  dB

Psat (measured at 50 MHz)  $\geq 27$  dBm

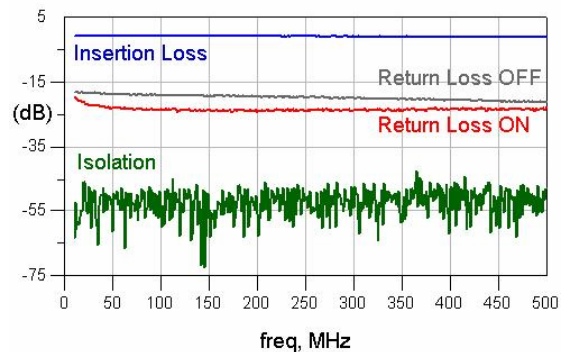


**Figure 4.8 Receiver Blanking Switch**

Low Noise Amplifier (LNA)

The receiver-blanking switch is followed by a low-noise amplifier to reduce the amount of noise introduced into the system. The selection of the amplifier was based on its noise figure, high gain and high saturation point. The gain and noise figure of this amplifier dictates the overall noise figure of the receiver. The saturation

point of the amplifier should be high to reduce the time of receiver blanking and avoid saturation from switch transients. High reverse isolation would minimize the power of multiples generated due to the non-ideal nature of the input impedance of components following the amplifier.

AS293 (Cougar Corp)

Gain  $\geq 28$  dB

Psat  $\geq 17$  dBm

Noise Figure = 2 dB

Reverse Isolation  $\geq 34$ dB

Input/Output Return Loss  $\geq 12$ dB

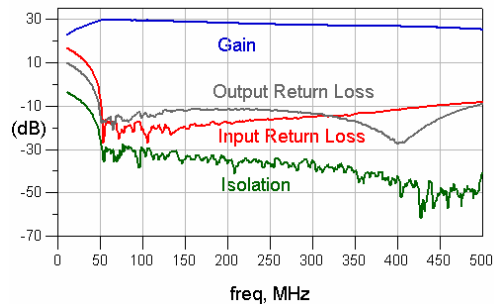


**Figure 4.9 Low Noise Amplifier**

### Bandpass Filter

Noise, which gets coupled through the first wideband bandpass filter, and harmonics and spurious signals generated by the LNA are removed by a bandpass filter with a narrow band and steeper roll off placed after the LNA. The filter has a 3-dB passband from 50 MHz to 200 MHz, thus providing inferior return loss characteristics at the edges of the passband. Poor return loss at the edges of the passband will generate reflections, but the reverse isolation provided by the LNA will stop these reflections from being transmitted back through the receive antenna to generate multiples. The price paid for steeper roll off is lower input return loss.

801124 (Bree Engineering)

Passband Insertion Loss  $\leq 0.6$  dB

Input/Output Return Loss  $\geq 17$  dB

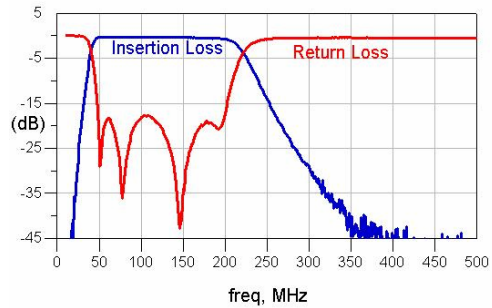


**Figure 4.10 Bandpass Filter**

### 20 dB Coupler

At the end of the front-end module, the signal is split into two parts by a 20-dB coupler and fed into both the gain channels. Using a 20-dB coupler instead of a power divider minimizes the receiver blanking time by preventing the LGC from saturating. A 20-dB coupler provides low mainline loss, thus minimizing the effective attenuation leading to high gain channel. The power divider was selected on the basis of providing low mainline loss with minimum variation.

ADC-20-4 (Minicircuits)

Mainline Loss  $\leq 0.4$  dB

Coupling  $\leq 19.5$  dB

Directivity  $\leq 21.2$  dB

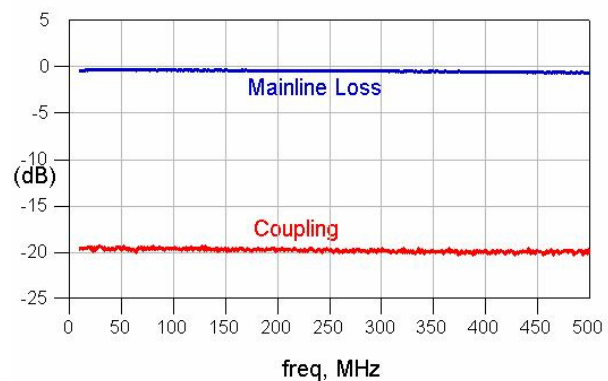


**Figure 4.11 Coupler (20 dB)**

Schematic and board image of the Front End module are shown below.

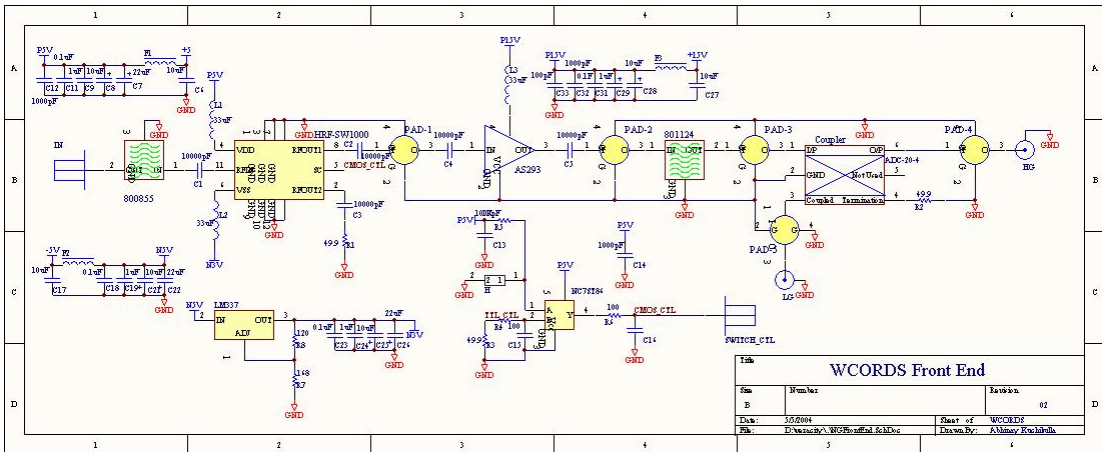


**Figure 4.12 Receiver Front End Schematic**

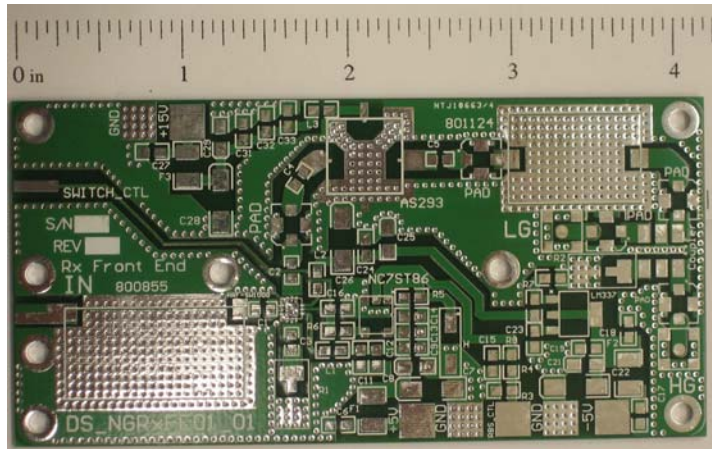


**Figure 4.13 Receiver Front End Board**

#### 4.4.2 High Gain Channel

Weak return signals from the bedrock and deep internal layers have to be amplified enough to fall into the dynamic range of the ADC. The product of effective gain in the Front End module and HGC should be high enough to push the receiver noise floor up to the ADC noise floor after including the integration gain. As

calculated in Chapter 3, the receiver gain with 1000 coherent integrations should be more than 48 dB.

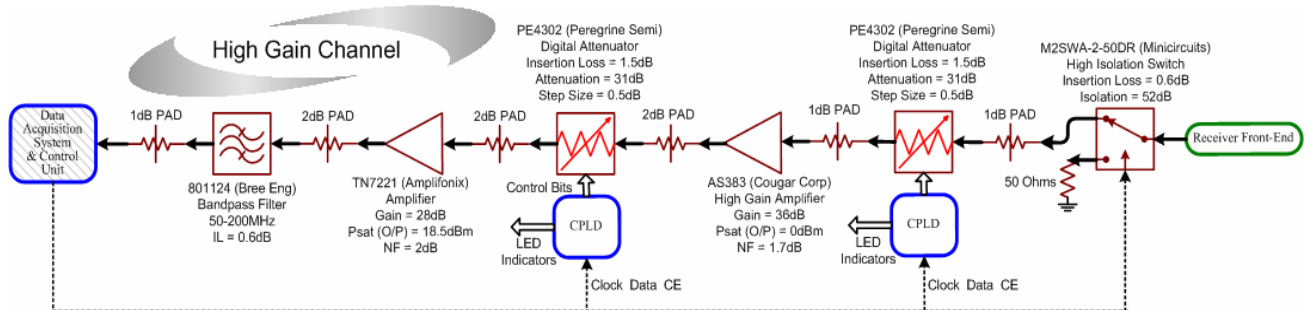


**Figure 4.14 High Gain Channel Block Diagram**

### High Gain Blanking Switch

When receiving high amplitude signals from the top and the shallow internal layers, which are being captured by the LGC, a high isolation switch shuts off the HG channel to avoid saturation. A SPDT HG blanking switch was selected to provide maximum isolation and small video leakage, and to be capable of operating above the saturation point of the LNA.

M3SWMA (Mini Circuits)

Insertion Loss ON  $\leq 0.6$  dB

Isolation  $\geq 52$  dB

Input Return Loss ON  $\geq 26$  dB

Psat  $\geq 20$  dBm

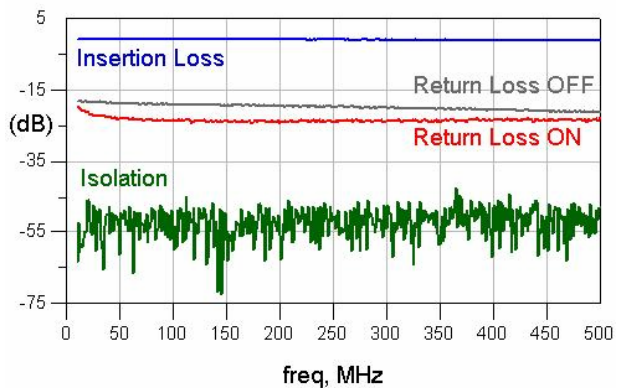


**Figure 4.15 High Gain Blanking Switch**

## Digital Attenuator

The gain in the receiver should have the capability of being varied to account for the following conditions:

- When radar is operated over a narrow band or in step frequency mode, the gain requirement changes
- The number of coherent integrations could be varied depending on the operating conditions, thus requiring variable gain

Different operating conditions require different receiver characteristics like gain and blanking time. The blanking time can be easily set with the control signal generated by a programmable FPGA in the control unit. The effective gain provided in the HGC can be varied using digital attenuators. Splitting the total attenuation between two digital attenuators would avoid increasing the effective noise figure of the system and also obtain maximum possible gain.

PE4302 (Peregrine Semi)  
Insertion Loss  $\leq 1.5$  dB  
Attenuation range = 31.5 dB  
Step Size = 0.5 dB



**Figure 4.16 Digital Attenuator**

Ideally, the gain of the HG channel is set such that at no instance in time ADC and amplifiers saturate. A CPLD is used to drive the 6 control bits on each digital

attenuator to set the required attenuation. The CPLD transforms the serial data from the control unit into parallel data to set the attenuation on the digital attenuator and provide control signals for the bi-level LEDs.

### High Gain Amplifier

Two amplifiers are being used in the HGC to obtain the required effective gain. The amplifiers were selected on the basis of providing large gain and have a saturation point below the absolute maximum input power of the amplifier and digital attenuator following it

AS383 (Cougar Corp)

Gain  $\geq 36$  dB

Psat  $\geq 0$  dBm

Input Return Loss  $\geq 12$  dB

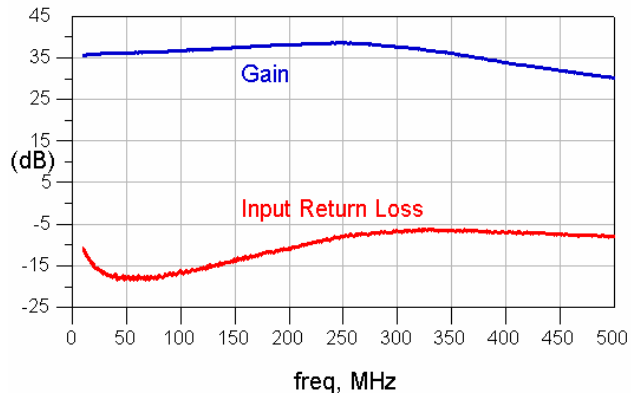


Figure 4.17 High Gain Amplifier

### Final Amplifier

This amplifier was selected such that it provides high gain and has a 1-dB saturation point larger than that of the ADC to compensate for the loss in passive components that follow the amplifier. Finally, the signal is passed through a bandpass filter to remove any spurious signals introduced by the amplifiers and the digital attenuators.

TN7221 (Amplifonix)

Gain  $\geq 28.5$  dB

Psat  $\geq 18.5$  dBm

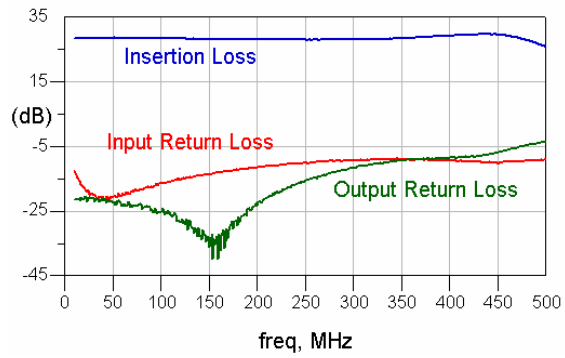


Figure 4.18 Final Amplifier

Fixed attenuators are placed in between components to avoid any oscillations due to improper matching. The schematic and board images are shown below:

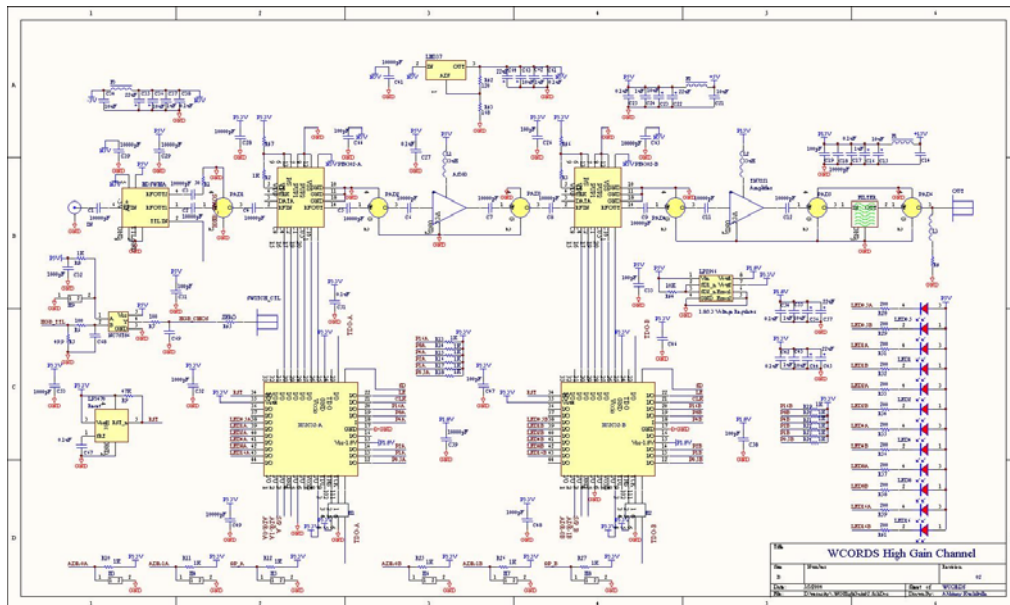
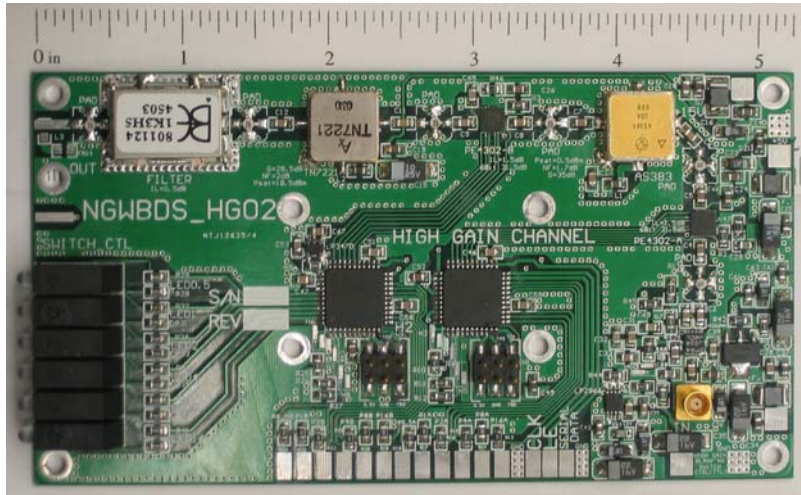
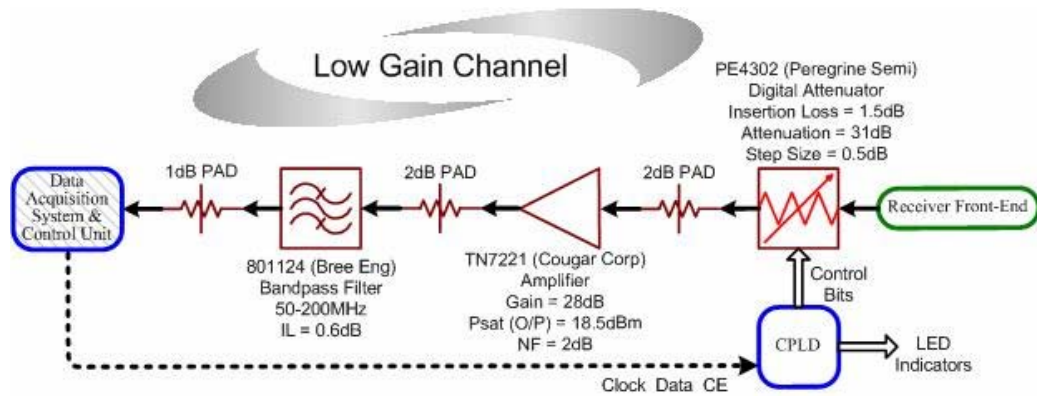


Figure 4.19 High Gain Channel Schematic



**Figure 4.20 High Gain Channel Board**

#### 4.4.3 Low Gain Channel



**Figure 4.21 WOCRDS Low Gain Channel**

The received signal from the top and shallow internal layers has large amplitude and requires little or no amplification to fall into the dynamic range of the ADC. Even though the receiver-blanking switch provides high isolation, the signal strength is large enough to cause the ADC to saturate if amplified in excess. As calculated in Chapter 3, gain in excess of 31.3 dB would saturate the ADC when

receiving the reflection from the top surface. The amplification provided by the LNA in the front-end module is almost nullified by the losses in the 20-dB coupler and other passive components in the front-end module. Any amplification required, should be provided in the LGC. Ability to vary the amplification in the receiver would allow the radar to operate in different operating conditions. The LGC block diagram, schematic and image of the board are given below.

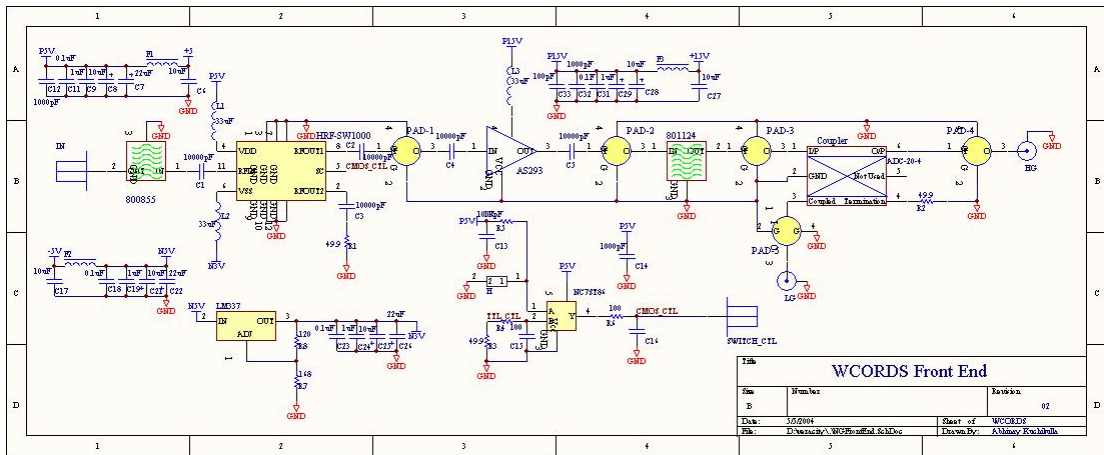


**Figure 4.22 Low Gain Channel Schematic**

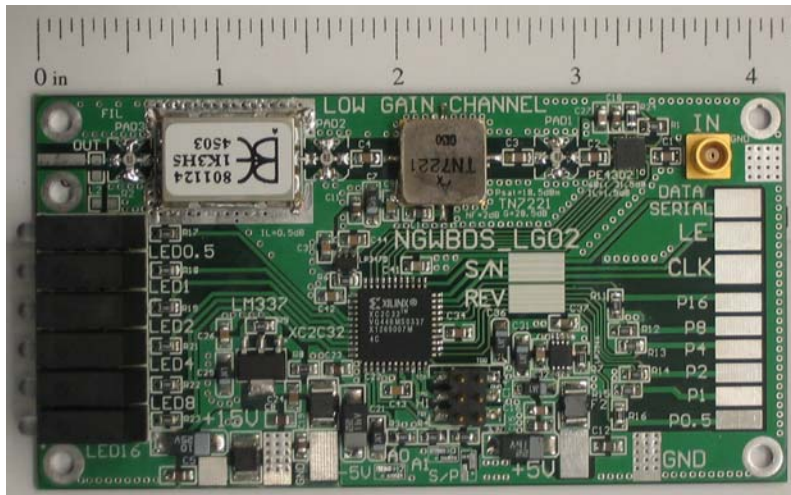


**Figure 4.23 Low Gain Channel Board**

The design of the LGC is similar to that of the HGC except for the exclusion of the blanking switch, high gain amplifier and a digital attenuator

#### 4.5 Frequency Synthesizer (10 MHz to 500 MHz)

According to the Nyquist theorem, the sampling rate must be at least twice the highest frequency component of the signal. Thus, generating or capturing a 200 MHz analog signal would require a sampling rate higher than 400 MHz to satisfy the Nyquist theorem. Sampling at 500 MHz would provide a guard band of 50 MHz thus minimizing the amount of noise being coupled back into the passband due to aliasing. The 500-MHz clock has to be phase locked to a 10-MHz stable reference clock to simplify the synchronization requirements with other radars and communication systems that are being operated simultaneously.

The Phase Lock Loop (PLL) chip (LMX 2326, National Semiconductors) divides both the 10-MHz reference clock and the signal from a Voltage-Controlled Oscillator (VCO) to a small reference frequency and passes them through a phase comparator. Depending on the phase difference between the two clocks, the phase comparator accordingly tunes the VCO output to the required 500-MHz clock and keeps it locked to that frequency. The PLL chip is designed by the manufacturer to operate over a wide frequency range, so the chip needs to be programmed for it to operate with selective frequencies. The data in the three volatile memory registers on the PLL chip define the reference comparison frequency and functionality of the chip. As the memory on the PLL chip is volatile, every time power is applied to the chip, it

needs to be programmed. A small CPLD with non-volatile memory is being used to program the PLL every time power is applied to the system.

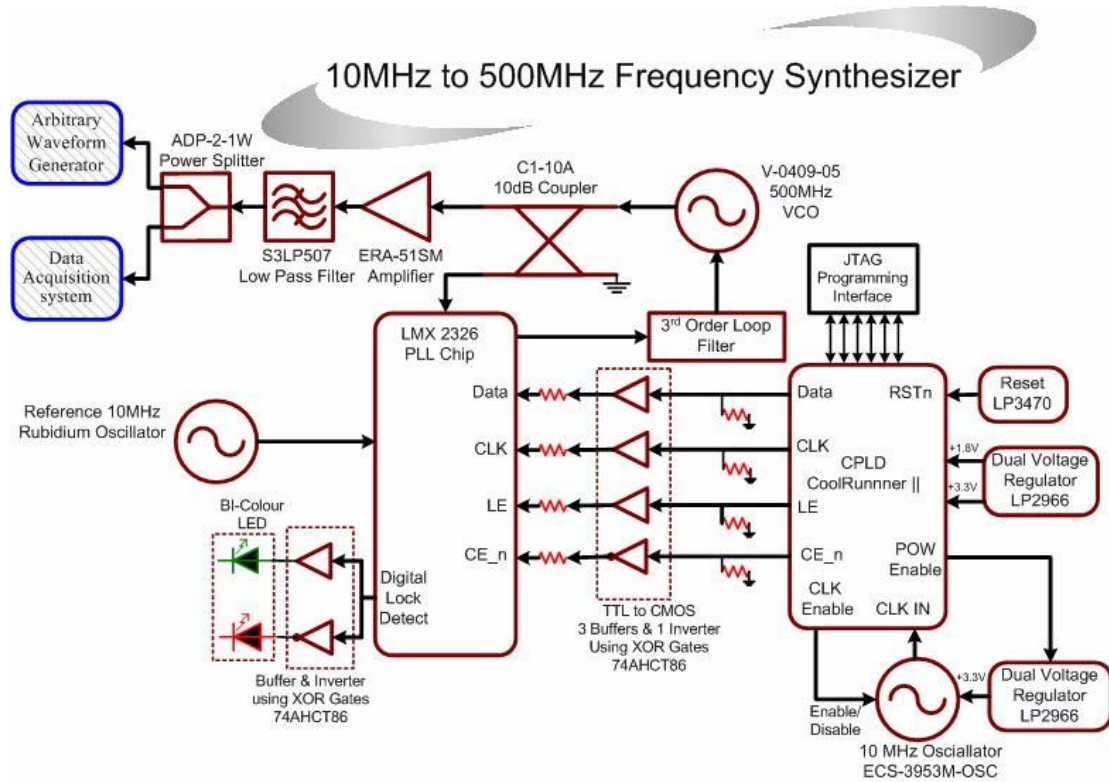


**Figure 4.24 10 MHz to 500 MHz Frequency Synthesizer**

When power is applied to the system, the following sequence of steps takes place to program the PLL chip

- Two dual voltage regulators power on the CPLD and an onboard 10-MHz programming clock
- After a predefined amount of time, a reset pulse is applied to the CPLD to initiate the programming sequence
- Data is serially loaded into all the three registers on the PLL chip at half the clock rate of the 10-MHz programming clock (5 MHz)

- Once the programming is finished, the PLL chip is enabled
- The 10-MHz programming clock is disabled and power to it is also turned off

Each programming line is passed through an XOR gate for transformation of voltage levels and data inversion. Once the PLL chip is programmed, it divides both the 10-MHz reference clock and signal out of the VCO to a reference frequency for phase comparison and tuning the VCO through the loop filter. The phase-locked 500-MHz clock is amplified and filtered to suppress harmonics before being divided in two by a power splitter to feed the waveform generator and data acquisition system. The schematic and image of the board are shown in Figures 4.25 and 4.26.

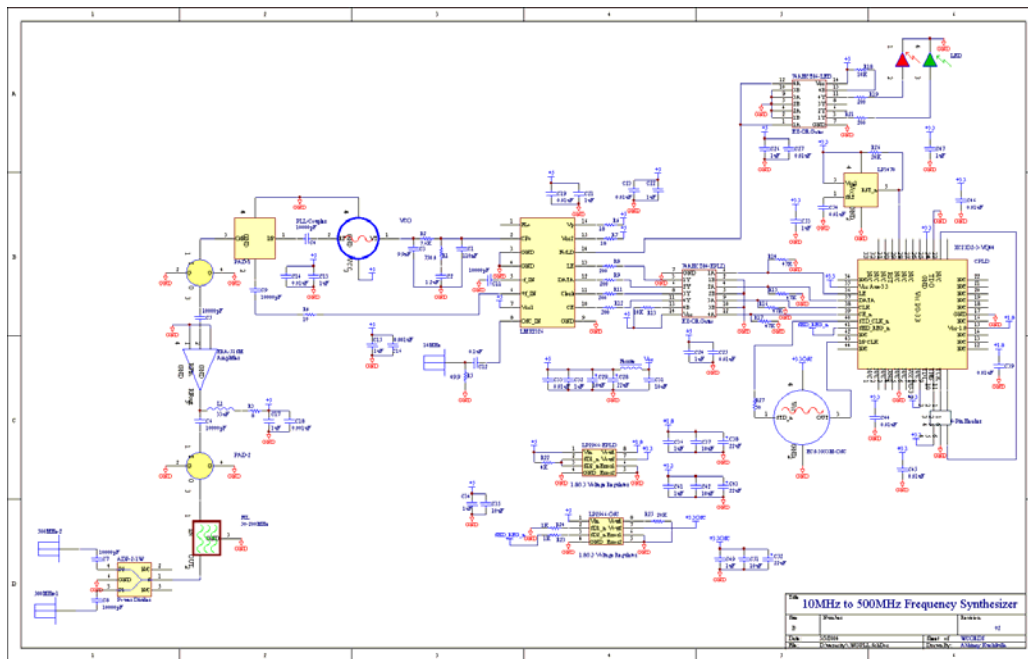


**Figure 4.25 10-MHz to 500-MHz Frequency Synthesizer Schematic**

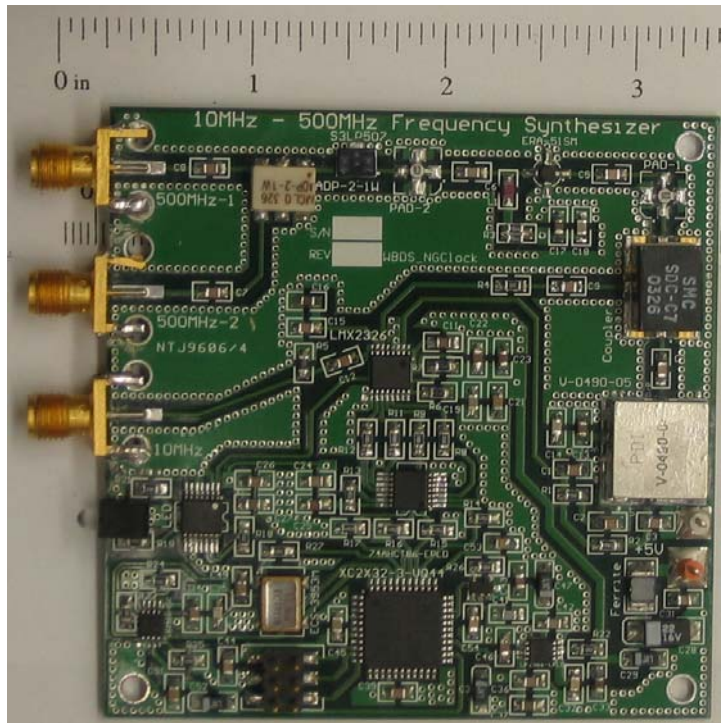


Figure 4.26 10-MHz to 500-MHz Frequency Synthesizer Board

# Chapter 5

## *System Housing and Results*

### 5.1 WCORDS Prototype

Initially, a prototype of WCORDS was designed and tested to validate the concept and discover any unseen problems with the radar. In-band interference caused due to noise from the digital system prevented the radar from being tested and collecting data over NGRIP during the 2003 summer field experiment. Though the system was not entirely successful in the field, a loop back test performed in the laboratory using a fiber optic delay line confirmed proper working of the radar in a noise free environment. The prototype of WCORDS was housed in an 18'' x 24'' x 7'' rack mount chassis along with a triple-output (+15 V, +5 V, -5 V) linear power supply. Each module was placed in an individual RF interference shielded enclosure. Modules were connected internally using mini-bend SMA cables. All the digital control signals for the switches and digital attenuators are routed through an interface card mounted on the front panel. SMA and type-N connectors on the front panel are used to interface all the analog signals going into and out of the radar. Copies of all digital control signals are routed out through the SMA connectors on the front panel for reference and testing. Based on the prototype, the final version of WCORDS was designed and developed. A significant number of modifications were done on the

prototype to optimize the radar to fit into compact PCI cards and improve its performance. The PCB boards used in the prototype had to be considerably miniaturized and designed to fit into compact PCI cards. Some of the components used in the prototype were replaced with better ones to improve the performance. Digital logic chips, such as CPLD's and XOR gates, were included on the boards to provide flexibility and simplify radar control logic. The degree to which the radar was miniaturized can be seen from Figure 5.1.

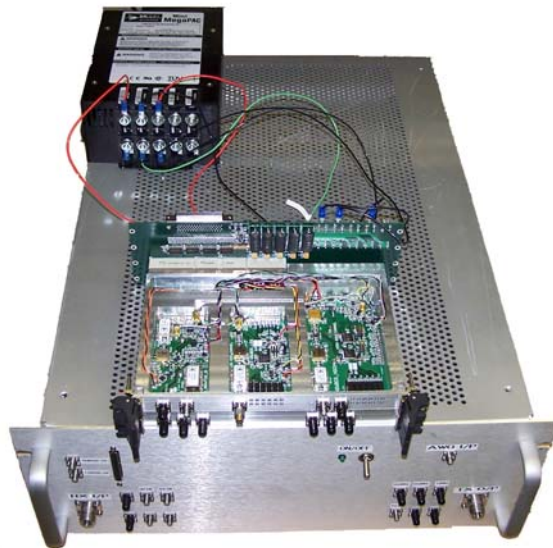


**Figure 5.1 WCORDS Prototype and the final version**

## 5.2 System Housing

The radar was designed to fit into two compact PCI cards made of aluminum. Cavities were milled on the compact PCI cards and boards were placed inside them. The thickness of compact PCI cards is just 0.5-0.6 inches, and after accounting for the space required for a 62mil board and base of the card, the maximum height

requirement for any component was restricted to just 0.45-5 inches. While selecting components for the radar, height limitation was also considered. The solid aluminum base to which the modules are attached provides good grounding among modules and acts as an excellent heat sink. Based on an approximate estimate of the size of each board, it was decided that two compact PCI cards were required to fit all the boards.

The following issues were addressed while designing the boards

- Provide the power input close to the end of the board to ease the routing architecture on the compact PCI card
- Provide good exposed ground plane on the back side of the board for proper grounding and good heat dissipation
- Appropriately place the analog inputs and outputs on the receiver boards to provide easy and small route for the SMA cables on the compact PCI card
- Provide good power filtering on the board to reduce the amount of switching noise coupling into analog signal
- Carefully select the dimensions of the boards for optimum fit

Channels were drilled on the compact PCI cards to allow power lines and analog SMA cables to pass through. The transmitter and the clock boards were placed on the first card and the second card carried the receiver boards. Bulkhead SMA connectors were used to route all the analog signal ports (Tx IN, Tx OUT, 10MHz IN, 500MHz OUT Tx, 500MHz OUT Rx, Rx IN, HGRx OUT and LGRx OUT) going into and out of compact PCI cards. Apart from analog signals, copies of the digital control signals

that are being fed from the backplane are also routed through to the front through SMA connectors for reference and testing. CPLDs on the HGC and LGC boards are used to program the digital attenuators and drive the LEDs.

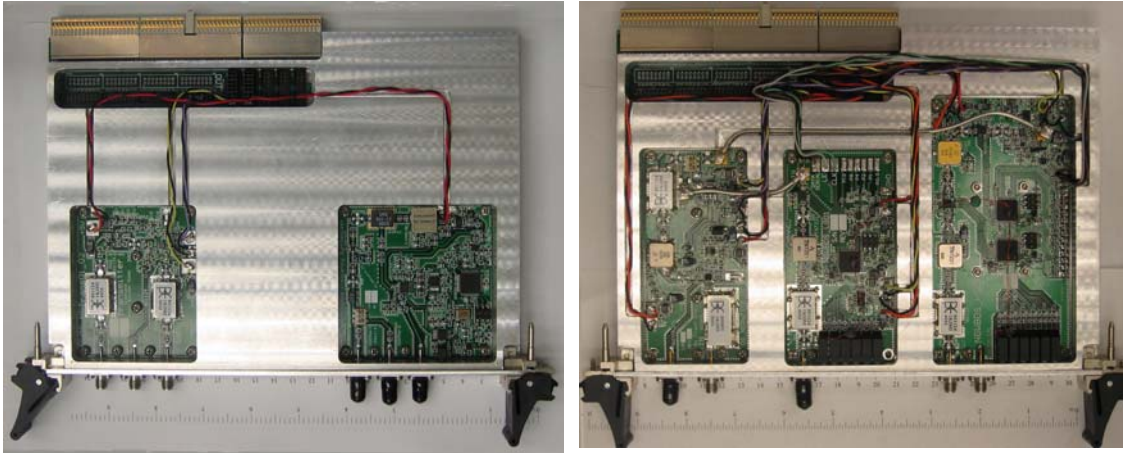


**Figure 5.2 WCORDS modules mounted inside Aluminum compact PCI cards**



**Figure 5.3 Transmitter and Receiver compact PCI cards mounted inside Euro Cage**

Both the cards are placed inside a euro cage that carries all the radars, data acquisition systems, signal generators, control units, 10MHz stable reference

oscillator and power supply. Power and control signals to the radar are fed through a backplane of the euro cage.

## 5.3 Results

### 5.3.1 Transmitter and Receiver amplitude response

For each RF component used in the radar, an evaluation board was designed and S-parameters were recorded using a network analyzer. Advance Design System (ADS) can be used to simulate the real time performance of the radar using the S-parameter files of each individual component. Using S-parameter files, amplitude variation and phase nonlinearities produced by each individual component can be removed in post processing or compensated in the transmit waveform. S-parameters files of each component will be helpful in debugging errors during testing of the radar and they also provide a good estimate of padding required between two components. The simulated and measured response of each individual module will be discussed in the following subsection.

#### 5.3.1.1 Transmitter

The S-parameters of the transmitter were recorded with the transmitter-blanking switch in ON and OFF positions. A close match between the measured and simulated amplitude response of the transmitter was obtained. Simulated and measured amplitude response of the transmitter module is shown in Figure 5.4.

Measured Gain  $\geq 8$ dB

Measured Input Return Loss  $\geq 18.1$ dB

Measured Output Return Loss  $\geq 21.4$ dB

Simulated Gain  $\geq 7.6$ dB

Simulated Input Return Loss  $\geq 18.1$ dB

Simulated Output Return Loss  $\geq 16.6$ dB

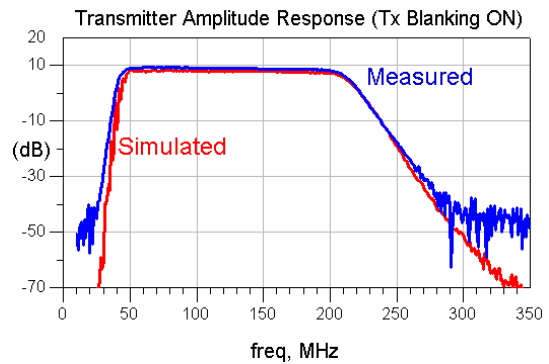


**Figure 5.4 Transmitter Amplitude Response with Tx Blk ON**

All the evaluation boards for the components were fabricated in-house using a milling machine, which introduces an error in obtaining exact trace dimensions. Small variations in S-parameters can be accounted for variation in characteristic impedance arising from errors in microstrip trace dimensions. Variation in board thickness could also contribute to the difference in simulated and measured results.

Measured Isolation  $\geq 41$ dB

Measured Input Return Loss  $\geq 19.2$ dB

Measured Output Return Loss  $\geq 19.7$ dB

Simulated Isolation  $\geq 45$ dB

Simulated Input Return Loss  $\geq 17.3$ dB

Simulated Output Return Loss  $\geq 19.8$ dB

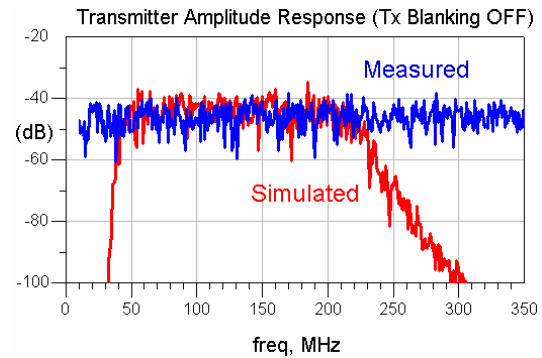


**Figure 5.5 Transmitter Amplitude Response with Tx Blk OFF**

The transmitter blanking switch in OFF state introduces around 50 dB of attenuation in the transmitter chain thus virtually shutting down the transmitter.

### 5.3.1.2 Receiver

The receiver input was terminated and the output of the HGC was measured on the spectrum analyzer to obtain the noise floor of the system as  $-88.5\text{dBm}$ . The amplitude response of the receiver can be analyzed under three different conditions

- Both receiver blanking and high gain blanking switched ON
- Receiver blanking switched OFF and high gain blanking switched ON
- Both receiver blanking and high gain blanking switched OFF

While transmitting, the direct feed through signal and return from the top are recorded at the output of LGC while switching both the receiver blanking and high gain blanking OFF, thus preventing the system from saturating.

Measured Isolation  $\geq 28.2\text{dB}$

Measured Input Return Loss  $\geq 16.7\text{dB}$

Simulated Isolation  $\geq 23\text{dB}$

Simulated Input Return Loss  $\geq 16.3\text{dB}$

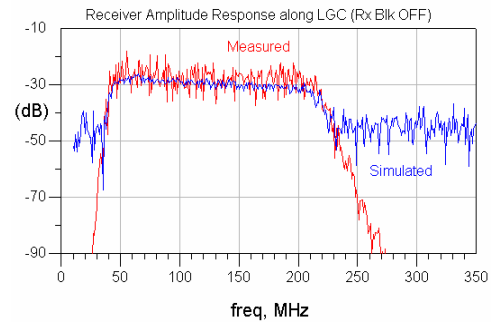


**Figure 5.6 Receiver Amplitude response with Rx and HG Blk OFF**

The medium power return signals from shallow internal layers are recorded at the output of the LGC while switching the receiver blanking OFF and high gain blanking ON, thus preventing the HGC from saturating.

Measured Gain  $\geq 24.5\text{dB}$

Measured Input Return Loss  $\geq 14.7\text{dB}$

Simulated Isolation  $\geq 23.4\text{dB}$

Simulated Input Return Loss  $\geq 15.8\text{dB}$

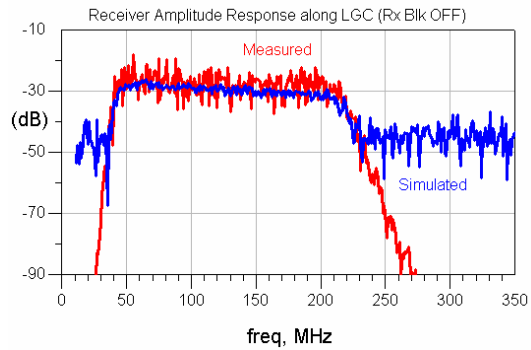


**Figure 5.7 Receiver Amplitude response with Rx Blk ON and HG Blk OFF**

The weak return signals from the bedrock and deep internal layers are amplified by the HGC and recorded at its output while having both the receiver blanking and high gain blanking OFF, thus providing maximum possible gain.

Measured Gain  $\geq 72.5\text{dB}$

Measured Input Return Loss  $\geq 16.7\text{dB}$

Simulated Isolation  $\geq 72\text{dB}$

Simulated Input Return Loss  $\geq 16.3\text{dB}$

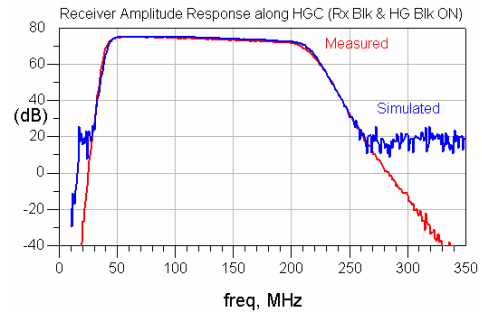


**Figure 5.8 Receiver Amplitude response with Rx and HG Blk OFF**

### 5.3.2 Transients

Video transients are generated in switches while the control signals are changing states. Though these transients last for a very short period of time, they can saturate components following the switch. The energy of these transients is spread over a wide frequency band, so including a bandpass filter just after the switch

reduces their effect. A slower transition rate between control states can reduce the amplitude of transients.

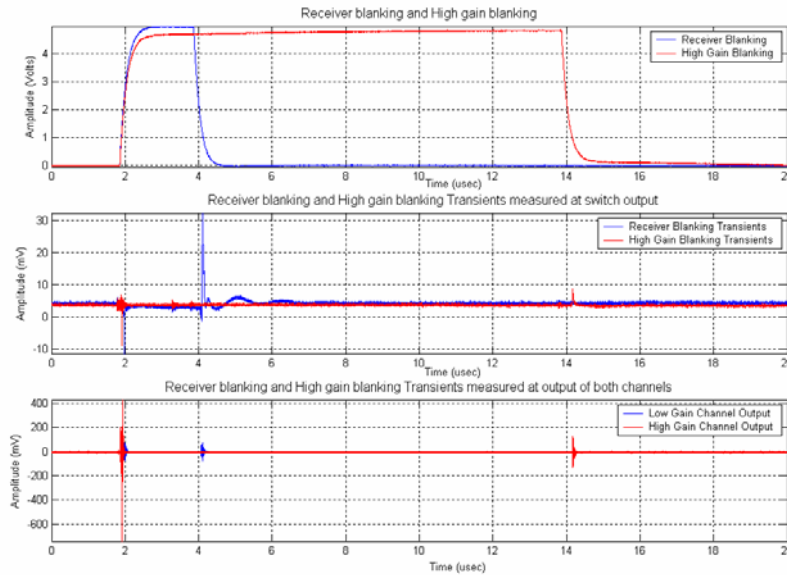


**Figure 5.9 Receiver Transients**

Both the receiver blanking and high gain blanking switch OFF at the same instant of time. The receiver blanking switches ON first, followed by the high gain blanking. The amplitudes of transients measured at the output of the switching are tabulated in Table

TRANSIENT	TIME	AMPLITUDE
Rx ON	2μsec	16mV (-31.9dBm in a 50Ω system)
HG ON	2μsec	14mV (-33dBm in a 50Ω system)
Rx OFF	4μsec	34mV (-25dBm in a 50Ω system)
HG OFF	14μsec	4mV (-44dBm in a 50Ω system)

**Table 5-1 Amplitude of Transients generated due to switching**

None of the transients is big enough to saturate amplifiers that immediately follow the switches. But, the transient noise generated when the receiver blanking switches OFF gets amplified along the HGC to saturate the A/D in the data acquisition system. This is caused because the high gain blanking switch takes more time to turn OFF than the receiver blanking switch. This problem can be easily resolved by switching OFF the high gain blanking a few clock cycles ahead of the receiver blanking.

### 5.3.3 Radar Pulse Compression

A loopback test was performed on the WCORDS to analyze the radar performance and correct the amplitude and phase nonlinearities introduced by radar. The AWG was programmed to generate a 50-MHz to 200-MHz linear chirp over a 1- $\mu$ sec period. The chirp was first passed through the transmitter module and then through the LCF power amplifier to be amplified to a peak power of 50W. The output of the power amplifier was connected to high power fixed attenuators to decrease the signal amplitude by 40dB. The signal is further attenuated by 70dB before feeding into the receiver. The signal at the output of both the gain channels is digitized and recorded on an oscilloscope at 2Gsp/s. Transmit chirp at the output of the AWG and receive chirp at the output of HGC are shown in Figure 5.10 and Figure 5.11. The output of LGC looks pretty same as the HGC output but at lower amplitude, so it is not being included.

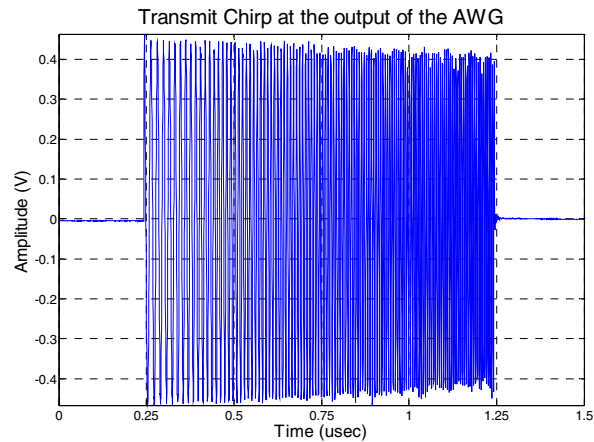


**Figure 5.10 Transmit Chirp at the output of the AWG**

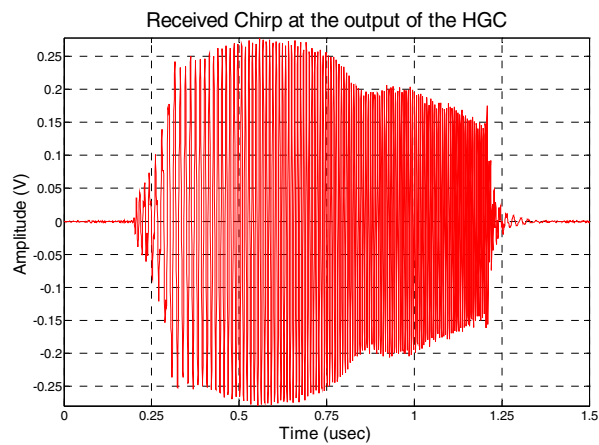


**Figure 5.11 Received Chirp at the output of the HGC**

Radar pulse compression is implemented using match filtering on the host computer. Matched filtering is achieved in the frequency domain when the spectra of the digitized and the conjugate of ideal reference chirps are multiplied [36]. These steps followed in implementing pulse compression are given as follows:

- The recorded signal is down converted to baseband using a quadrature mixer mixer

- The upper sideband and the higher-order harmonics are later filtered using a low-pass filter
- The baseband signal in time domain is transformed to frequency domain using the Fast Frequency Transform (FFT). The FFT process transforms both time-domain signals into the frequency domain
- An ideal baseband chirp from DC to 75MHz is generated and appropriate weighting is applied to it
- The weighted ideal baseband chirp is transformed to frequency domain using FFT
- Both the ideal and recorded signals are multiplied in frequency domain and transformed into time domain using the Inverse Fourier Frequency Transform (IFFT)

The IFFT process of the multiplication gives the compressed baseband chirp with a pulse width of  $1/B$  (6.66 nsec). A Hanning window was used as it has the first sidelobe 31dB lower to main lobe and has faster sidelobe roll off characteristics. It was noticed that the amplitude and phase response was varying with the input power, so the power amplifier was disconnected while recording data for analyzing the pulse compression results.

The received waveform and its impulse response are shown in Figure 5.12:

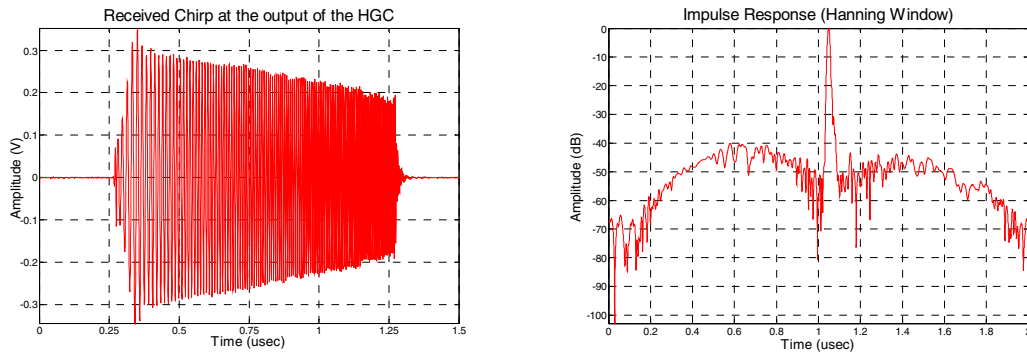


**Figure 5.12 Received chirp and its Impulse response**

Due to the phase and amplitude nonlinearities introduced by the components in the radar system, the impulse response has higher and uneven sidelobes. The first sidelobe is 10dB higher than the ideal value. The impulse response of both ideal (recorded at the output of AWG) and the received signals is shown in Figure 5.13

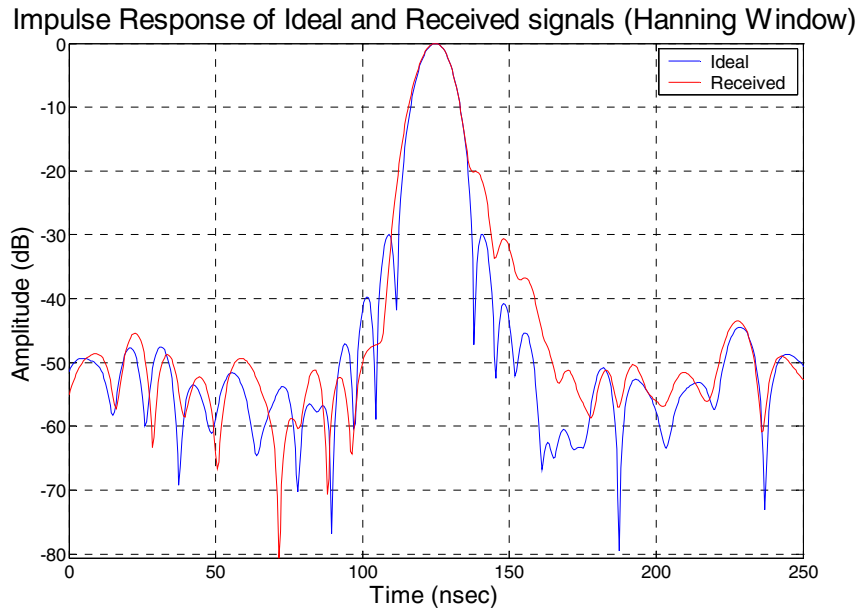


**Figure 5.13 Impulse response of ideal and recorded signals**

The amplitude and phase nonlinearities introduced by the system were inverted and introduced into the transmit chirp generated by the AWG. The amplitude and phase corrected transmit and received chirps are shown in Figure 5.14.

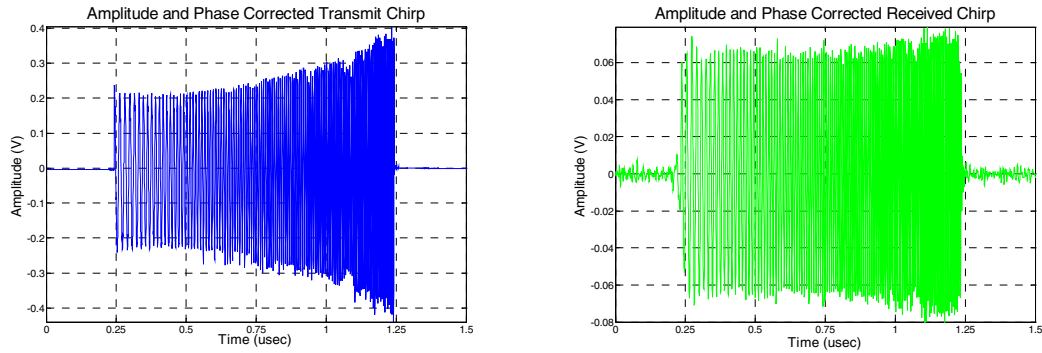


**Figure 5.14 Amplitude and Phase corrected transmit and received signal**

After implementing amplitude and phase correction, the sidelobe performance improves considerably, by 8.5 dB. Impulse responses of the ideal, un-corrected and corrected signals are shown in Figure 5.15

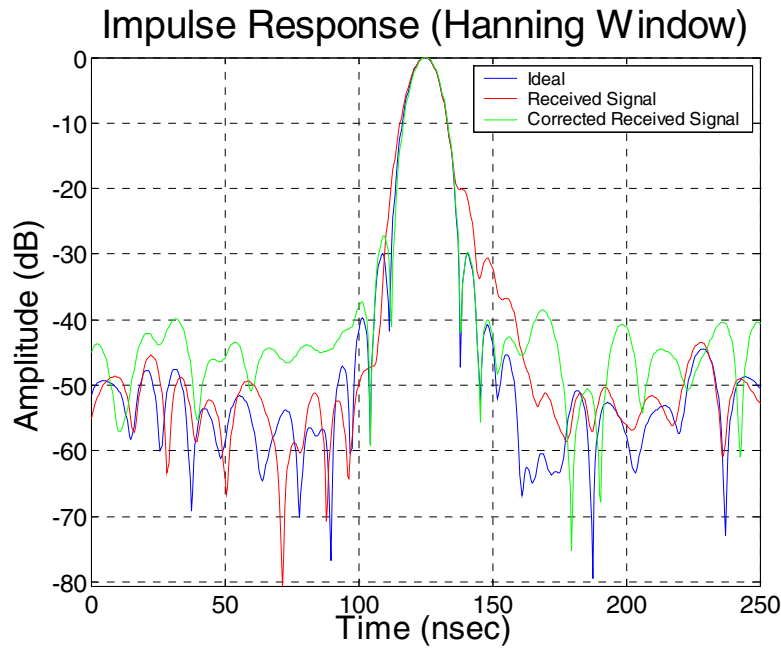


**Figure 5.15 Impulse response of ideal, un-corrected and corrected signals**

The maximum sidelobe level for ideal, un-corrected and corrected waveforms is tabulated in Table 5.2.

SIGNAL (HANNING WINDOW)	RELATIVE SIDELOBE LEVEL
Ideal Hanning	31dB
Signal at the output of the AWG	30dB
Received Signal without applying any correction	20dB
Amplitude and Phase Corrected Received signal	27.5dB

**Table 5-2 Sidelobe performance**

### 5.3.4 Clock

The frequency response of the 10-MHz to 500-MHz frequency synthesizer was measured using a spectrum analyzer, and the power measured at its tuned frequency and harmonics is tabulated in Table 5.3

FREQUENCY	POWER
500MHz	5.68dBm
1GHz (1 <sup>st</sup> Harmonic)	32.28dBc
1.5GHz(2 <sup>nd</sup> Harmonic)	50.68dBc
2GHz(3 <sup>rd</sup> Harmonic)	68.7dBc
2.5GHz(4 <sup>th</sup> Harmonic)	70dBc

**Table 5-3 Frequency Synthesizer performance**

# Chapter 6

## Conclusions and Future Recommendations

### 6.1 Conclusions

The WCORDS system was designed and developed to meet the objectives and requirements of the PRISM project. The radar can be operated over the entire band from 50 MHz to 200 MHz. A prototype was initially designed and tested before developing the final radar system. An AWG is used to generate the required transmit chirp within selectable pulse widths. The transmitter was implemented on a two-layer board with dimensions 3" × 2.4". The amplification provided by the transmitter is sufficient to drive the power amplifier to generate 80W of peak power.

The receiver was split into three different modules to provide good isolation and simplify the design. The front-end module of the receiver was implemented on a two-layer board with dimensions 4" × 2". The front-end module was designed to have a small noise figure and good reverse isolation. Providing dual channels in the receiver considerably increased the effective dynamic range of the receiver. The maximum effective gain through HGC of the receiver is 75dB and can be varied by 63dB with a resolution of 0.5dB. The HGC of the receiver was implemented on a four-layer board with dimensions of 5" × 2.6". CPLDs and other digital logic components used on the boards simplify the control logic used to alter the receiver

parameters. The LGC was implemented on a four-layer board with dimensions of  $3.9'' \times 1.9''$ .

The 10Mhz to 500MHz frequency synthesizer provides a clean and stable clock to the waveform generator and the data acquisition system. The clock system was implemented on a  $3'' \times 3''$  four-layer board. Considerable improvement in the sidelobe levels was noticed after including the phase and amplitude nonlinearities in the transmit pulse. Summarized below are some important characteristics of the radar

- Ability to detect ice thickness up to 4km
- Map deep internal layers with a resolution of 56cm
- Obtain important information about ice sheet basal properties and scattering characteristics over a wide frequency range
- Small and compact

The WCORDS system will be mounted inside an automated rover and tested in Greenland during the 2004 field season.

## 6.2 Future Recommendations

Power amplifiers for the land based (50W) and airborne (200W) operation are mounted inside rack mount chassis, which makes the entire system big, heavy and unwieldy. Highly efficient and linear class E power amplifiers can be designed to output 200W and fit on a single compact PCI card. Another possible solution that can be adopted is to divide the transmit signal into multiple channels and amplify the signal in each channel using small and readily available power amplifiers. The output

of each power amplifier can be fed into single or multiple elements of an antenna array.

Better resolution can be obtained if the radar is operated over a wider band. With the advent of recently developed wideband antennas and with few modifications to the radar and the data acquisition system, the radar can be operated up to 400 MHz. And as calculated in chapter 3, the loss through ice is pretty much constant over the frequency band 50 MHz to 400 MHz.

As the radar hasn't been tested in the field, at this point in time, not many improvements regarding system operation can be suggested.

## References

- [1] Gogineni, S., PRISM proposal report (unpublished), 2000-2002
- [2] James, G.T. and Vijay Narayanan. "The Probability of Sea level rise," Library of U.S. Global Change Research Information Center, September 1995.
- [3] Hollin, J.T. and R.G.Barry, "Empirical and Theoretical Evidence Concerning the Response of the Earth's Ice and Snow Cover to a Global Temperature Increase," *Environmental International* vol. 2, pp 437-44, 1979.
- [4] Goodwin, I., and C.Bentley, "ISMASS," U.S. Geological Survey ISMASS 2255 N. Gemini Dr., Flagstaff, AZ ([www.ancrc.utas.edu.au/scar/ismass.html](http://www.ancrc.utas.edu.au/scar/ismass.html)).
- [5] Chuah, T.S., "Design and Development of a Coherent Radar Depth Sounder for Measurement of Greenland Ice Sheet Thickness," RSL Technical. Report 10470-5, January 1997.
- [6] Saikiran, P.V.Namburi, "Design and Development of an Advanced Coherent Radar Depth Sounder," RSL Technical Report, 2003.
- [7] Gogineni, S., T.S. Chuah, C. Allen, K. Jezek, and R.K. Moore, "An improved coherent radar dept sounder," *Journal of Glaciology*, vol. 44, no. 148, pp. 659-669, 1998.
- [8] Waite, A.H. and S.J Schmidt, "Gross errors in height indication from pulsed radar altimeter operating over thick ice or snow," *Institute of Radio Engineers International Conventional Record*, no 5, pp. 38-53.

- [9] Robin, G. de Q., "Polar ice sheets: a review," *Polar Rec*, vol. 16, no. 100, pp. 5-22.
- [10] Drewry, D.J., "Comparison of electromagnetic and seismic-gravity ice thickness measurements in East Antarctica," *J.Glaciol*, vol. 15, no. 73, pp. 137-150, 1975.
- [11] Raju, G, "Coherent Antarctic Radar Depth Sounder (CARDS): Design, Development and Results," PhD Dissertation, University of Kansas, School of Engineering, 1989.
- [12] Sinsheimer, R.L. "Altitude determination," in Hall, J.S., ed., *Radar aids to navigation*, New York, McGraw-Hill, pp. 131-142, 1947.
- [13] Walfol, M.E.R., "Radio echo sounding through ice shelf," *Nature*, vol. 204, no. 4956, pp. 317-319, 1964.
- [14] Fedorov, B.A., "Primeneniye aktivnoy radiolokatsii dly izucheniya antarkticheskikh lednikov [Radar sounding of Antarctica ice]," *Inf. Byull. Sov. Antarkt. Eksped*, vol. 62, pp. 19-24, 1967.
- [15] Rinker, J.N., and S.J. Mock, "Radar ice thickness profiles – northwest Greenland," CRREL Spec Rep 103, 1967.
- [16] Evans, S., "Progress report on radio echo sounding," *Polar Rec.*, vol. 13, no. 85, pp. 413-420, 1967.
- [17] Evans, S., ed., "Review of radio echo system performance in Gudmandsen, P.E.," Proceedings of the International Meeting on Radioglaciology, Lyngby, Denmark, pp. 100-102, 1970.

- [18] Evans, S., and B.M.E. Smith, "A radio echo equipment for depth sounding in polar ice sheets," *Journal of Physics*. E, Ser.2, vol. 2, pp.131-136, 1969.
- [19] Jazek, K., "Radar measurement of borehole geometry on the Greenland and Antarctica ice sheets," *Geophysics*, vol. 50, no. 2, pp. 242-251, 1985.
- [20] Bjornsson, H., R.L. Ferrari, K.J. Miller and G. Owen, "A 1976 radio echo sounding expedition to the Vatnajokull ice cap, Iceland," *Polar Rec*, vol. 18, no. 15, pp. 375-377, 1977.
- [21] Sverrisson, M., E. Johannesson and H. Bjornsson, "Radio-echo equipment for depth sounding of temperate glaciers," *Journal of Glaciol*, vol. 25, no. 93, pp. 477-486, 1980.
- [22] Allen, C., "Parameters of Time-Domain Radio Depth Sounder Systems reported in the literature," University of Kansas, unpublished, 1996.
- [23] Fujita, S.; Matsuoka, T.; Ishida, T.; Matsuoka, K.; and Mae, S., "A summary of complex dielectric permittivity of ice in the megahertz range and its applications for radar sounding of polar ice sheets," *International Symposium on Physics of Ice Core Records*, Shikotsukohan, Japan, Sept. 14-17, pp. 185-212, 1998.
- [24] Demarest, K.R., "*Engineering Electromagnetics*," Prentice Hall, Inc., New Jersey, ISBN: 0023285214, 1998.
- [25] Matzler, C. and U.J. Wegmuller, "Dielectric properties of freshwater ice at microwave frequencies," *Applied Physics*, vol. 20, no. 12, pp. 1623-1630, 1987.

- [26] Matsuoka, T., S. Fujita, and S. Mae, "Effect of temperature on dielectric properties of ice in the range 5-39 GHz," *Journal of Applied Physics*, vol 80, no 10, pp. 5884-5890, Nov. 15, 1996.
- [27] Ulaby, F.T., R.K. Moore, and A.K Fung, *Microwave Remote Sensing vol. III*, Artech House, Norwood, MA, 1986.
- [28] Robin, G. de Q. S. Evans and J.T Bailey, "Interpretation of radio echo sounding in polar ice sheets," *Philosophical Transactions of Royal Society*, London, vol. A256, no. 1166, pp. 437-505, 1969.
- [29] Tiuri, M.E., A.H. Sihvola, E.G Nyfors and M.T. Hallikainen, "The complex dielectric constant of snow at microwave frequencies," *IEEE Journal of Oceanic Engineering*, oe-9, pp. 377-382, 1984.
- [30] Glen, J.W. and J.G. Paren, "The electrical properties of snow and ice," *Journal of Glaciol*, vol.15, no. 73, pp. 15-38, 1975.
- [31] Paden, J., C.T. Allen, S.P. Gogineni, D. Dahl-Jensen, L.B. Larsen, and K.C. Jezek, "Wideband Measurements of Basal Scattering and Ice Sheet Attenuation," (submitted), *TGARS* 2003-2004.
- [32] Wolff, E.W., "Nitrate in polar ice," *Journal of Geophysics Res.* 100, pp. 16249-16264, 1995.
- [33] Ewen B.M. Smith and S. Evans, "Radio echo sounding: Absorbtion and Scattering by Water inclusion and Ice Lenses," *Journal of Glaciol*, vol. 11, no 61, pp. 133-147, 1972.

- [34] Stratton, J.A., *Electromagnetic Theory*, McGraw-Hill Book Co, ASIN: 0070621500, 1941.
- [35] Matzler, C. and U.J. Wegmuller, *Applied Physics*, vol 20, pp 1623-1630, 1987.
- [36] Wehner, D.R., *High-resolution radar*, second ed., Artech House, Inc., Norwood, Massachusetts, 1995
- [37] Henslee, J., "Antenna Design for polar ice radars," RSL Technical Report, 2003.